Titanium Dioxide in Chromogenic Devices: Synthesis, Toxicological Issues, and Fabrication Methods

Valeria De Matteis [1] [ID], **Alessandro Cannavale** [2,3,*] [ID] **and Ubaldo Ayr** [2]

[1] Department of Mathematics and Physics "Ennio De Giorgi", University of Salento, Via per Arnesano, 73100 Lecce, Italy; valeria.dematteis@unisalento.it

[2] Department of Sciences in Civil Engineering and Architecture, Polytechnic University of Bari, 70125 Bari, Italy; Ubaldo.Ayr@poliba.it

[3] Istituto di Nanotecnologia, CNR Nanotec, Via Arnesano 16, 73100 Lecce, Italy

[*] Correspondence: alessandro.cannavale@poliba.it

Abstract: The use of titanium dioxide (TiO_2) within two specific classes of devices, namely electrochromic and photoelectrochromic, is described hereafter, with respect to its inherent properties and chromogenic features within architectures that have appeared so far, in this field. The new research trends, involving the applications of TiO_2 in chromogenic materials are reported, with particular attention paid to the techniques used for film deposition as well as the synthesis of nanoparticles. Furthermore, the main studies concerning its chemical-physical properties and approaches to its chemical syntheses and fabrication are reviewed, with special regard to "green" routes. In addition, the main aspects relating to toxicological profiles are exposed, with reference to nanoparticles and thin films.

Keywords: titanium dioxide; synthetic approaches; toxicity; chromogenic devices

1. Introduction

Titanium dioxide (TiO_2) is a well-known photocatalyst and anti-microbial metal oxide material, which is widely used in many commercial products [1]. A yearly production of 10,000 metric tons has been estimated [2], mainly for nanosized TiO_2. TiO_2 nanoparticles (NPs) are used in a wide range of applications due to their strong photocatalytic activity [3]. In addition, their white color is particularly suitable for enhancing opacity in paints, plastics, food additives, and cosmetics [4–6]. The ability of TiO_2 to filter UV-A wavelength radiation justifies its use in sunscreens [7]. Other types of applications for TiO_2 are water treatment, due to its purification capability [8], and self-cleaning coatings for surfaces [9]. Its use in chromogenic devices and materials will be investigated in this work,

TiO_2 NPs exhibit excellent catalytic behavior; the electronic energy levels, in a semiconductor, constitute energy bands, hereafter designated as Valence Band (VB) and Conduction Band (CB), unconnected by a band gap. When an electron in the VB captures an energy amount greater than the band gap, it can be promoted to the CB, leaving a positive hole in the VB. When the electron hole (e^- h^+) pair is produced, it can move towards the semiconductor surface, triggering several redox reactions with chemical species adsorbed on the semiconductor surface, contributing to the photocatalytic reaction [5,10]. The thermodynamic properties of its band structure are the basis of its photocatalytic performance [11].

When surfaces are exposed to UV light, TiO_2 produces Reactive Oxygen Species (ROS) such as hydroxyl radicals and super oxide ions. When the size decreases at the nanoscale, the catalytic activity is dramatically enhanced [12]. TiO_2 mainly exists in three widely studied crystalline forms; namely, anatase (tetragonal with a bandgap of 3.3 eV), rutile (tetragonal with a bandgap 3.1 eV), and

brookite (orthorhombic); each one shows different photocatalytic activity due to distinct electronic band structures and mass density [13]. Anatase and rutile forms are constituted by chains of distorted TiO_6 octahedra, where each Titanium (Ti) atom is surrounded by six oxygen atoms [14]. The synthesis of brookite is difficult; for this reason, its application is limited. In general, the initial crystalline phase is anatase, which is quickly converted into the rutile phase after calcination (600 °C); the process is irreversible due to the bonds breaking and reforming. The brookite form can be transformed into the rutile phase by heating it at 800 °C. Rutile is the most chemically stable of the three phases, with a melting point between 1830 °C and 1850 °C [15], in accordance with thermodynamic calculations [16]. The most investigated TiO_2 phase forms for photocatalytic applications are anatase and rutile; they present a bandgap equal to 3.20 eV and 3.02 eV, respectively. Anatase shows larger photo-catalytic activity due to its more negative conduction band edge potential (higher potential energy of photo generated electrons) and high specific area and photochemical stability [17].

When TiO_2 is exposed to UV radiation ($\lambda = 384 \div 410$ nm), $e^- h^+$ carriers are generated and redox reactions can occur with chemical elements, such as water, Nitric Oxide (NOx), Sulfur Oxide (SOx), Ammonia (NH_3), Hydrogen Sulphide (H_2S), Hydroxide (OH^-) ions, Carbon monoxide (CO), and Carbon dioxide (CO_2), that are absorbed on the TiO_2 surface [16].

The photocatalytic behavior of TiO_2 has been understood since the early 19th century, and it was not long after, in the 1970s, that Fujishima and Honda proposed the use of TiO_2 powders for the photoelectrolysis of water [18]. After UV exposure, the created holes (h^+) in the VB oxidize H_2O or OH^- ions to the hydroxyl radical ($OH^\bullet$); at the same time, the electrons promoted in the CB reduce the adsorbed O_2 species to a superoxide ($O_2^\bullet$), triggering a series of chemical reactions that lead to the production of $OH^\bullet$ radicals. These radicals react with organic substances, degrading them into H_2O and CO_2.

TiO_2 nanomaterials can show different shapes and sizes, and this influences their numerous applications; for example, nanotubes [19] and nanorods [20] are more suitable for dye-sensitized solar cells than nanospheres. In general, the physico-chemical properties of TiO_2 NPs depend on the synthetic route. "Top-down" and "bottom-up" approaches are commonly used to obtain NPs. The top-down approach is based on the breaking of the bulk material into smaller particles by using different techniques such as sputtering and thermal/laser ablation whereas, in the bottom-up approach, NPs are synthesized using chemical and biological methods by the self-assembly of atoms [21].

Different techniques are suitable for the synthesis of TiO_2 NPs and fabrication of TiO_2-based devices: sol-gel, chemical and physical vapor deposition (CVD and PVD) techniques [22–24], sono-chemical and microwave-assisted methods, hydrothermal and oxidation routes [25], spray pyrolysis [26–28], wet chemical techniques [29,30], doctor blading [31], and anodization [32].

Moreover, in the last few years, the so called "green" routes have received great attention due to their use of non-toxic solvents and their reproducibility with easily scalable processes [33].

2. Synthetic Routes and Fabrication Techniques for TiO_2

2.1. Sol-Gel

The sol-gel method is a colloidal chemical technique, extensively used to synthetize large quantities of metal oxide NPs at low temperature (<100 °C), with an accurate control of size and shape. In the first step, the precursor monomers (metal oxides and metal chlorides) are converted into a colloidal solution (sol) by hydrolysis; the sol acts as the precursor for gel formation, which forms particles or polymers. The precursors are hydrolysed and poly-condensed to obtain colloids [34] (Figure 1). In detail, metal alkoxides contain M-O-R bonds (M is the metal, O is oxygen, and R is the alkyl group). Hydrolysis starts with a nucleophilic attack on the M-O bonds and a consequent nucleophilic substitution reaction, in the presence of water, which replaces the O-R bonds in the O-H groups. The condensation step occurs when the OH^- groups develop a metal oxide network and build small nuclei [35]; in addition, the possibility to customize the route allows for the design of different shapes of TiO_2, applying

several steps in the synthetic process [36]. The addition of chelating ligands, such as carboxylic acids, β-diketones, or acetylacetone, in the sol-gel route permit the acquisition of sols and gels with specific properties. For example, the use of β-diketones leads to the formation of smaller particles; these chemical species act as capping and polymerization agents. One of the disadvantages of sol-gel is the low purity of products that require long post-synthesis treatment [37].
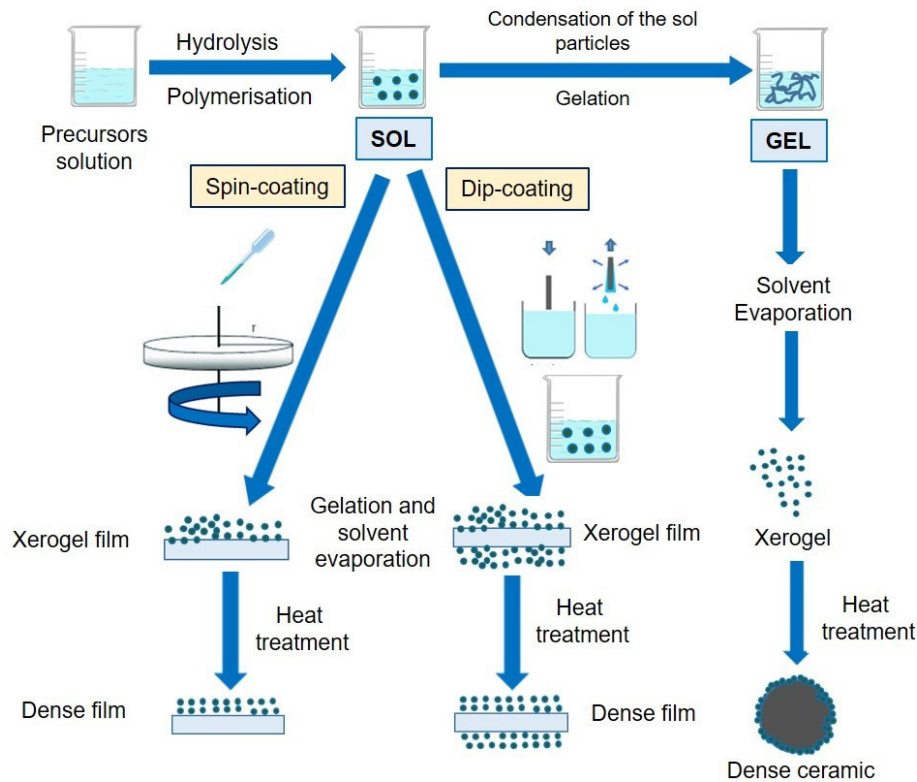
Figure 1. Schematic representation of the typical sol-gel route.

The sol-gel method is a versatile alternative for producing TiO_2 films [38,39]. As already specified in Section 2.1, the hydrolysis of specific precursors (such as metal alkoxides $M(OR)_4$) produces the so-called "sol" and then a "gel", according to the following reactions of hydrolysis and condensation:

$$\textbf{Hydrolysis: } M(OR)_n + nH_2O \rightarrow M(OH)_n + nROH \tag{1}$$

$$\textbf{Condensation: } M(OH)_n \rightarrow MO_{\frac{n}{2}} + \left(\frac{n}{2}\right)H_2O \tag{2}$$
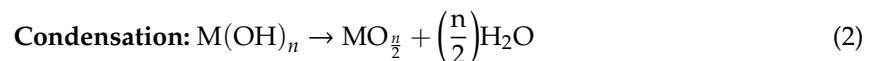
It has been observed that the color of TiO_2 in the dark state depends on the precursor used; you will have grey colored states if Titanium tetra-n-butoxide is used and blue colored states by adding acetic acid to the alkoxide precursor before the hydrolysis steps in [40]. Eventually, a gel is obtained when solvents undergo complete evaporation and polymerization takes place. In the case of TiO_2, an amorphous xerogel is obtained, as confirmed by X-ray diffraction analysis; eventually, it may turn into crystalline anatase at about 673 K [40]. Sol-gel is a facile synthetic approach at room temperature, allowing for low-cost deposition techniques, such as spin-coating or dip-coating, leading to the fabrication of a dense, ceramic material. Tetraisopropoxide was reported as a suitable precursor for both mesoporous and nanoporous TiO_2 films [41]. Dinh et al. [42] investigated the electrochromic (EC) properties of films fabricated using a sol-gel dipping method. Zhang et al. [43] adopted the sol-gel technique to fabricate a solid-state EC device embodying TiO_2 and a solid polyelectrolyte, reporting transmittance modulation of 27.3%. The highest performance was obtained in the infrared region. The highest coloration efficiency (CE) of 79.4 cm^2/C was measured at 1000 nm; visible modulation

was lower (16% at 560 nm). This work highlights the potential role of TiO_2 as a cathodic EC material especially devoted to infrared modulation.

Wu et al. [44] prepared EC TiO_2, starting from a dispersion of NPs of different sizes. Their NP_S-based films were deposited on a transparent conductive oxide (TCO) by dip-coating using different process rates (from 1000 to 3000 µm/s). Afterwards, the films underwent sintering by heating them at 500 °C for half an hour. The authors observed the dependence of EC figures of merit on thickness and roughness of the deposited films. Furthermore, they found that higher EC performance was obtained by using NPs with a smaller diameter; 5 nm TiO_2 gave modulations of 27.0% whereas 100 nm NPs gave just 16.9%.

In a recent work, TiO_2 NPs were achieved by sol-gel method using different concentrations of tetra isopropyl orthotitanate (TIP) at room temperature. The anatase and rutile mixed powder was obtained after drying and calcination processes conducted at 500 °C. The SEM analysis showed a spongy morphology and some agglomeration phenomena. In addition, the authors measured an optical band-gap in the range of 2.7 to 3.12 eV; this result indicated that the photo-activity occurred in the near visible region and shows that obtained TiO_2 NP_S may be suitable for several kinds of application [45]. Singh et al. [46] obtained TiO_2 NP_S by the non-hydrolytic sol-gel route using $TiCl_4$ and benzyl alcohol with high band-gap and absorption in the visible light region. These NPs were used in an electron-transporting layer using a low-temperature deposition process on perovskite solar cells, showing a high efficiency (18.97%) on the glass and 13.51% on flexible plastic substrates. Titanium tetraisopropoxide (TTIP) in water-in-oil micellar solutions of water/cyclohexane/Triton X-100 was adopted to synthesize anatase TiO_2 NPs by a hydrolysis-condensation process. In this way, the authors obtained small NPs with a particle size of 10–15 nm, due to the gradual hydrolysis of titanium alkoxide [47].

2.2. Chemical Vapor Deposition (CVD) and Physical Vapor Deposition (PVD)

The vapor deposition technique is based on the vaporization of a certain material from a source, assisted by high temperature, vacuum, gaseous plasma. Eventually, the vapor condenses onto the substrate to generate solid thin films. The process can be chemical (CVD) or physical (PVD) [48].

CVD is a deposition route widely used to achieve thin films made of crystalline or amorphous compounds, metal alloys, and semiconductors. In the CVD process, a volatile precursor, in the presence of some carrier gases (NH_3, H_2), induces the solid material formation at the atomic level in a reaction chamber, which finally is formed on a specific substrate. There are two factors that lead to different grain size and shape formation: substrate temperature and vapor supersaturation (Figure 2a). These two parameters impact the rate of the film formation and the nucleation rate, respectively [49,50].

In particular, the growth of a single crystal on a substrate is promoted by high temperature and low gas supersaturation. On the contrary, low substrate temperatures and high gas supersaturation boost the formation of amorphous film development as well as the polycrystalline formation [51]. There are some variant of CVD, such as Atomic Layer Deposition (ALD), in which the precursors are pulsed alternately, and they are introduced into the reaction chamber in order to obtain the material by chemical surface reactions [52]. Small TiO_2 NPs (<10 nm) were achieved using a helium/oxygen atmosphere mixed to TTIP by pyrolysis. In addition, TiO_2 films (30 nm) can also be obtained with the same conditions, as demonstrated by Seifried et al. [53]. TiO_2 nanorods (50–100 nm) were obtained by metal organic CVD (MOCVD) using TTIP as a precursor [54]. TiO_2 nanorods can be synthetized on silica substrates by the MOCVD route using titanium acetylacetonate ($Ti(C_{10}H_{14}O_5)$). The latter is vaporized in the low-temperature area of a furnace (200–230 °C) before being moved to the high-temperature zone, at 500–700 °C, by the gas carrier flow; finally, TiO_2 nanorods can be obtained directly on the substrates [55]. The thermal plasma synthesis permits the acquisition of highly pure products without the use of high vacuum and capping agents. Macwan et al. [56] obtained different sizes of pure TiO_2 NPs using different arc currents. The size ranged from 25 nm to 30 nm when the current was set at 80 A and from 30 nm to 42 nm with a current of 120 A. In a CVD typical process, Ti powder is

located on a quarts substrate in a tube furnace, and the temperature is increased to 850 °C in vacuum under argon flow, obtaining TiO_2 nanowires after 3 h [57,58]. A different CVD method was developed by Zhang et al. [59] in order to obtain pure anatase-phase TiO_2 films that were resistant and stable at high temperatures. The precursor was represented by TTIP, which was dissolved in ethanol at a concentration of 0.10 mol/L. The precursor was moved to a reaction chamber, where the substrate was heated at 400 °C using carrier gas and compressed air followed by a post-annealing treatment using high temperatures (600 to 1100 °C). The small crystalline anatase TiO_2 showed high thermal stability with a sheet-like grain structure.
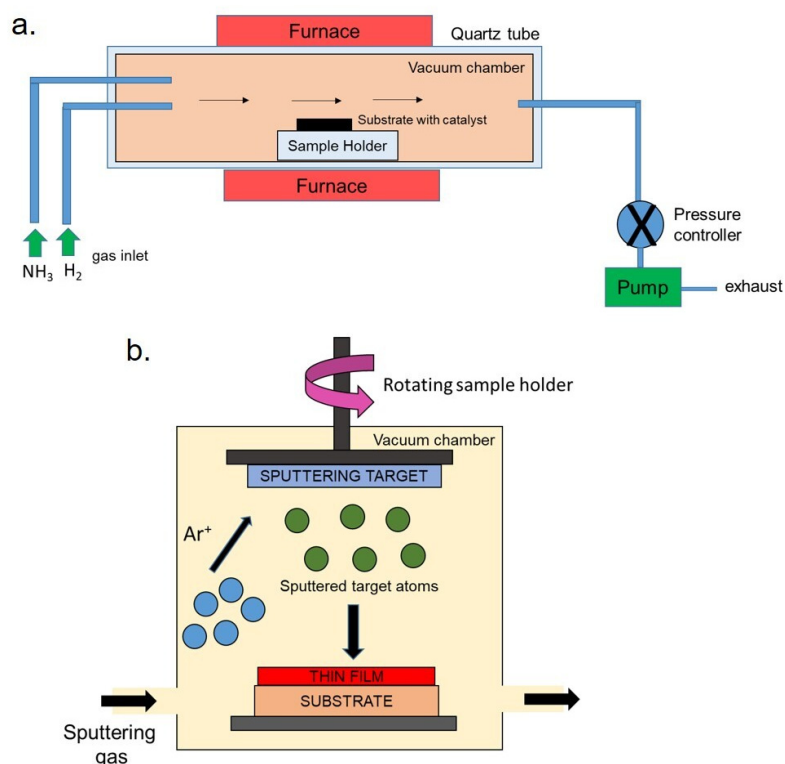
Figure 2. (**a**) Schematic representation of Chemical Vapor Deposition (CVD) and (**b**) Physical Vapor Deposition (PVD) processes.

Differently from the CVD route, in the PVD processes the precursor is not a gas but a solid material that can be deposited by its vaporization due to a high-energy source, such as an electron beam or sputtering [60]. The vapor generated is moved to a low-pressure area by gas (oxygen, nitrogen, or methane) or vacuum for its further condensation on the substrate, developing a thin film with a nanoscale thickness. The main PVD routes are: thermal evaporation, electron beam evaporation, sputtering, and ion plating [61]. Thermal evaporation is an approach mostly used in industrial fields to deposit a thin film by the formation and growth of a specific material under High Vacuum (HV) pressure and through different steps [62]. The target material is vaporized by applying high temperature, and successively the vapor is transported to the substrate by vacuum. This last step is characterized by the condensation of the material on a substrate, forming a thin film [63].

Ion plating technique is based on intermittent bombardment of a film by energetic flux ions, which controls the properties of the depositing film. The process takes place inside an inert gas discharge source where the gas pressure ranges from 1 to 0.1 Pa. The final product is a dense film suitable for depositing a hard-thin film on compound materials [64]. Contrary to thermal evaporation, generally the sputtering route does not require substrate heating to vaporize the solid material (Figure 2b) [65]. In fact, the atom escapes from the target materials by an atomic collision caused by argon or nitrogen plasma bombardment, and the substrates are placed in front of the target at an appropriate distance.

Finally, the target is vaporized and the vapors are deposited on the substrate, creating a thin atomic layer. The entire procedure takes place in a vacuum chamber in the presence of low pressure plasma (0.67 Pa) [66].

A largely used physical approach is reactive electron-beam evaporation, producing amorphous TiO_2 films (1 nm grain size) if the substrate temperature is kept below 300 °C during the fabrication process; substrate temperatures higher than 400 °C allow for the fabrication of anatase TiO_2 thin films. Sputtering has been widely used as to produce TiO_2 films. Reactive dc magnetron sputtering was used by Sorar et al. [67]. In their work, several 200 nm thick films were fabricated to fully assess the effects of the deposition parameters (i.e., the argon sputter gas pressure or oxygen to argon ratio) on their EC figures of merit. Sputtering allowed for the fabrication of highly performing films at room temperature. The same group also investigated the effect of the film thickness on EC properties, finding that the best CE (26.3 cm^2/C) can be observed in 400 nm thick films, fabricated at 25 °C with an oxygen/argon ratio of 0.04 [68].

Albeit these methods are consistent for obtaining good TiO_2 NPs, without the use of toxic chemicals their use is often unfeasible due to the limitations caused by large energy consumption, the need of expensive instrumentation, and long times required to reach thermal stability.

2.3. Sonochemical and Microwave-Assisted Methods

The sonochemical methods are used to develop TiO_2 NPs with high photocatalytic properties by the hydrolysis of TTIP in water or in a mix of ethanol/water under ultrasonic waves. Sonochemistry is based on the use of ultrasound with frequencies between 20 kHz and 2 MHz to induce physical, chemical, and thermal effects in solution [69]. This method includes three steps: formation, growth, and implosive collapse of microcavities in a liquid [70]. Cavitation collapse triggers intense local heating (~5000 K), high pressures (~1000 atm), and enormous heating and cooling rates (>109 K/s) reaching temperatures in the order of 5000 K [71].

The cavitation step can be generated by different physical phenomena such as high velocity rotation, Venturi, and high-pressure nozzles. The energy generated by these is converted into friction, waves, and cavitation [72].

Microwave-assisted synthesis is a green route suitable to the preparation of different product microspheres, gel beads, tablets, and thin films [73]. The microwaves are electromagnetic radiations with wavelength ranges from 0.01 to 1 m, which are particularly effective to induce nucleation or growth of material. The electromagnetic radiations induce an excitation of polar molecules by rotational and vibrational motion producing heat. The process is characterized by low energy consumption with respect to the electric furnaces widely used in CVD processes. In addition, the microwaves permit the acquisition of nanoproducts with a higher yield in a shorter time, with a controllable particle size and purity with respect to the other processes mentioned above [74].

In the microwave-assisted methods, the synthesis of TiO_2 NPs occurs by irradiation of microwaves with frequencies between 0.3 and 300 GHz. In general, this method is based on two steps, namely dipolar polarization and ionic conduction [75]. Due to the fast heat transfer, this route can be applied to synthesize TiO_2 NPs with a good size control and reproducibility in a short time process (from 5 min to 1 h). However, the decrease in reaction time and temperature induces limitations in the particle growth. In a work by Baldassarri et al. [76], anatase NPs were prepared in 30 min using titanium tetrachloride ($TiCl_4$) in H_2SO_4 aqueous solution, which was used to prevent the crystallization of brookite. Cabello et al. [77] proposed the fast synthesis of colloidal anatase by the microwave hydrothermal method, based on a sulphate esterification reaction and its application to the oxygen reduction reaction. The authors obtained a TiO_2 film on porous graphite substrates. Their catalytic activity was measured by means of cyclic voltammetry. The synthesis of anatase, brookite, and rutile TiO_2 NPs were obtained by a microwave-assisted hydrothermal method using amorphous TiO_2 as a starting material at different concentrations (0.05 M, 0.1 M, and 0.2 M) in HCl. The nanomaterials were obtained under hydrothermal conditions at 140 °C, 160 °C, 180 °C, and 200 °C and dried at

room temperature in order to have a final product after vacuum treatment [78]. Reeja-Jayan et al. [79] synthesized crystalline anatase TiO_2 thin films on indium tin oxide (ITO)-coated glass substrates that were immersed in a solution containing tetraethylene glycol (TEG) and a Ti-based sol-gel precursor. The mix was further heated at 150 °C in a microwave reactor to create a nucleation site for the TiO_2 film to grow on (Figure 3).
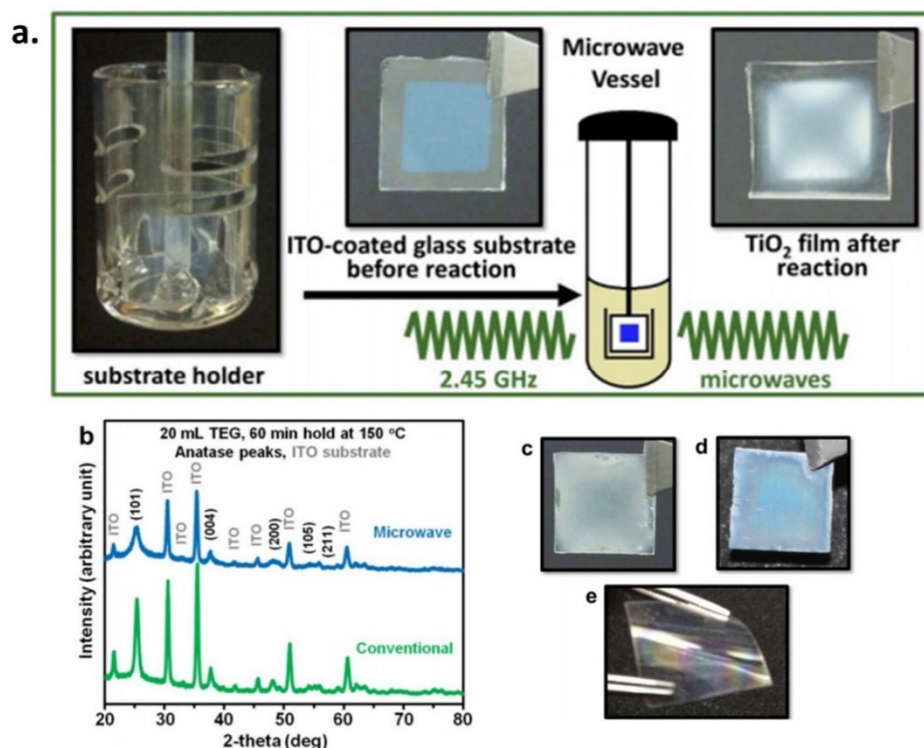
Figure 3. (**a**) Schematic representation of microwave reaction to grow thin titanium dioxide (TiO_2) film. (**b**) XRD spectra of TiO_2-indium tin oxide (ITO)-coated glass. The strong peaks were associated with the anatase phase, in particular the (101) peak. (**c**) Microwave-grown TiO_2 film on ITO-coated glass. (**d**) Microwave-grown TiO_2 film on Alluminium-coated glass. (**e**) Microwave-grown TiO_2 film on ITO-coated Polyethylene terephthalate (PET). Adapted from reference [79].

2.4. Hydrothermal Method

The hydrothermal route is a powerful tool to achieve stable nanomaterials, especially of transition-metal compounds. This method is based on the crystallization phenomenon of a certain material, caused by high vapor pressure and moderate temperature (about 300 °C) using an aqueous solution of the material. The process occurs in an autoclave at a pressure of about 10 bar.

In general, the solvent is water, and a metal hydroxide (e.g., NaOH) is added as a mineralizer. The metal salts or metal alkoxides are used as a source of metal ions. The first step is nucleation, followed by particle growth in order to obtain a specific particle-size distribution. The same procedure is required for the solvothermal method, differing only in the wetting liquid, which is usually an organic solvent [80].

The hydrothermal method is particularly suitable for synthesizing anatase, rutile, and mixtures of the rutile-anatase phases. Through this route, NPs with high purity and crystallinity can be obtained, but some factors, such as temperature, reaction time, and the medium influence the crystallization step. Reddy et al. [81] showed the synthesis of pure anatase and pure TiO_2, controlling the reaction conditions during the hydrothermal synthesis from $TiCl_4$. They obtained pure anatase (5–15 nm) at 120 °C and pure rutile (15–25 nm) at 250 °C, without additives. Despite the great advantages, including the possibility to obtain a nanotube morphology, this synthetic process requires long processing times,

high NaOH concentrations, and expensive equipment; in addition, the control of crystal growth is very hard. When the temperature is in the range between 100 °C and 200 °C, the crystallinity of TiO_2 nanotubes increases, but a prolonged time of reaction promotes morphological NPs alteration. On the other hand, the solvothermal route employs non-aqueous solvents and the reaction temperature can be enhanced, overcoming the limit of the specific boiling point characterizing liquid solvents. Kim et al. [82] used titanium isopropoxide (TIP) as a precursor to be decomposed by high temperature in the surfactant-dissolved toluene solution. The solution was heated at 250 °C for 20 h in autoclave in order to obtain small TiO_2 NPs (about 6 nm). When a greater amount of precursor was added, the shape of the nanomaterials turned in rods. Feng et al. [83] used a $TiCl_4$ solution saturated with NaCl at 160 °C for 2 h in order to obtain TiO_2 nanorods. The solvothermal method allows control of the shape, size, and crystallinity better than the hydrothermal method due to the higher control of titanium precursors, temperature, duration, and solvents [84]. Recently, pure anatase TiO_2 NPs with a small size (7.5 nm) were achieved using TIP and isopropanol by the hydrothermal method. The product was obtained after high temperature treatment (200 °C) in autoclave and following annealing at 350 °C [85]. Beyer et al. [86] reported a continuous hydrothermal flow route in order to obtain rutile TiO_2 nanorods with a temperature dependent tunable size (from 35 to 60 nm in length). Consequently, the bandgap ranged from 3.2 to 3.5 eV.

2.5. Oxidation Method

The oxidation route requires the oxidation of Ti via the use of anodization or oxidants. In a typical route, TiO_2 nanorods on a Ti plate were synthesized using a 30 wt% H_2O_2 solution at 353 K for 72 h. The formation of crystalline TiO_2 takes place by a dissolution precipitation mechanism. When inorganic salts (NaF, NaCl, $NaSO_4$) are added, the TiO_2 crystalline phase can be tuned; F and SO_4 addition promotes the anatase synthesis, while formation of rutile is boosted by Cl [87]. Nanotubes were synthetized from a Ti sheet under a voltage between 10 V and 20 V in hydrogen fluoride. Additionally, oxygen, argon, and acetone are used as sources of Ti oxidation [88]. Rutile TiO_2 nanowires were achieved by thermal oxidation of titanium foil via the use of potassium hydroxide (KOH) in two steps. First, the reduction of KOH into droplets at 400 °C followed the oxide growth at 500–800 °C in the furnace. The nanowires were obtained at high concentration and showed a length between 500 and 600 nm [89].

TiO_2 rutile monocrystalline nanowires by thermal oxidation were also btained by Arcadipane et al. [90], showing an improvement of photocatalytic activity compared to a reference TiO_2 bulk sample.

2.6. Spray Pyrolysis

Spray pyrolysis methods allow the formation of TiO_2 and TiO_2-based thin films in a one-step process, without further purifications or more drying steps [13–15]. This method is based on the aerosol formation from precursors (metallic salts or a colloidal solution), which are heated in a furnace at high temperature, favoring formation of micro particles with a specific size after many steps of evaporation, drying, and annealing [91] (Figure 4). Spray pyrolysis is a very simple and cost-effective processing method that permits the acquisition of high-quality substrates or chemicals. The method is also suitable for depositing dense, porous, and multilayered films, making it a powerful tool in the glass industry [8] and in solar cell production [92].
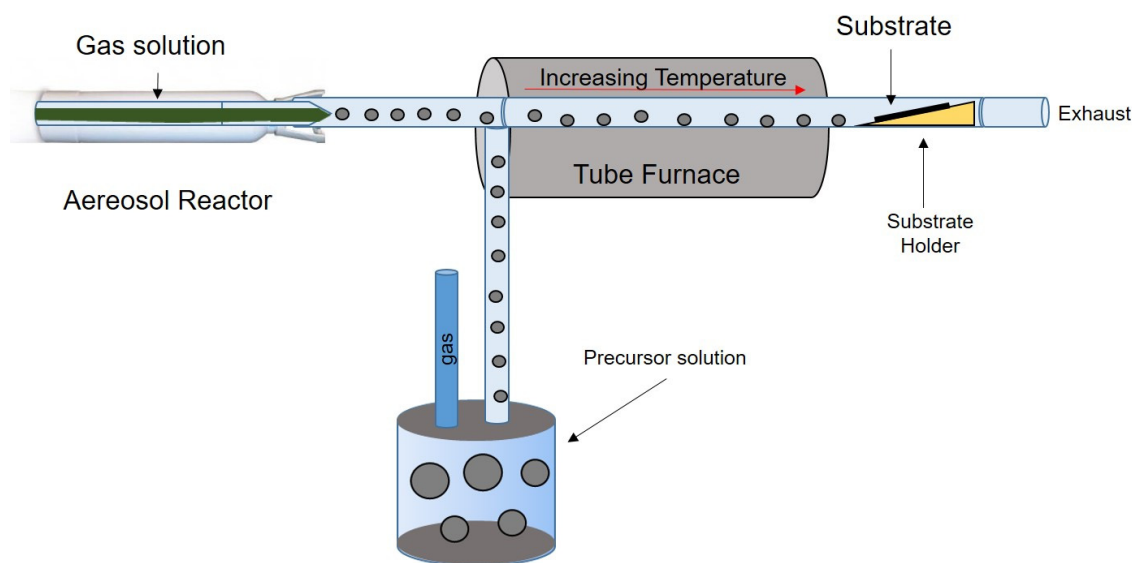
Figure 4. Schematic representation of a typical spray pyrolysis process.

Recently, Ramadhan et al. [93] synthesized WO_3 and TiO_2 NPs by one-step flame spray pyrolysis, for the applications in EC devices using TIP as a titanium precursor and ammonium metatungstate hydrate $((NH_4)_6H_2W_{12}O_{40} \cdot xH_2O,)$ as a tungstate precursor. Annealing of up to 1000 °C for 2 h was used to improve the NPs crystallinity in order to use them in EC devices (2 wt%), and it showed high transmittance as well as a fast kinetics. Wang et al. [94] obtained TiO_2 NPs directly from three organic precursors: TTIP, water-soluble titanium sources TC-300®, and TC-400® using the low-pressure spray pyrolysis route. Dense films of TiO_2 were deposited on F-doped SnO_2 substrate by spray pyrolysis and were used for several applications such as photocatalysts, sensors, and solar cell fabrication [95].

A molten salt-assisted pyrolysis process was achieved to obtain TiO_2 nanowires [96] from $TiCl_4$-ethyl acetate and Na_2S-ethyl acetate. Anatase TiO_2 nanowires were obtained after calcination at 820 °C while rutile TiO_2 nanowires were obtained at a higher temperature (970 °C).

2.7. The "Green" Route

The methods described above represent the most common methods used to synthesize high quality TiO_2 nanomaterials, but they unfortunately have several drawbacks. They often require the use of toxic chemicals and long purification processes after synthesis, along with high-energy consumption. In this framework, the so called "green chemistry" may represent an eco-friendly alternative to traditional methods due to the use of natural, non-toxic agents (usually plants, microorganisms, or fungi) [33]. In particular, in the plant extracts, fito-constituents such as flavonoids, alkaloids, terpenoids, and polyphenols act as reducing and capping agents of metallic/metal oxide solutions. Subhapriya et al. [97] described the biosynthesis of anatase TiO_2 NPs with a size ranging from 20 nm to 90 nm by using the aqueous leaf extract of *Trigonella foenum-graecum*, an aromatic leguminous plant widespread in many Middle Eastern, European, and Asian countries. In addition, the authors observed strong antimicrobial activity of TiO_2 on *Staphylococcus aureus*, *Enterococcus faecalis*, *Klebsiella pneumoniae*, *Streptococcus faecalis*, *Pseudomonas aeruginosa*, *Proteus vulgaris*, *Bacillus subtilis*, *Yersinia enterocolitica*, and the fungus, *Candida albicans*. Additionally, *Azadirachta indica* leaf extract was used by Thakur et al. [98] to produce spherical TiO_2, starting from an aqueous solution of Ti precursor. In the literature, other plants, such as *Nyctanthes arbortristis* [99], *Annona squamosa L.* [100], and *Echinacea purpurea* [101], were used to obtain TiO_2 NPs. In the future, green TiO_2NPs may be used to fabricate chromogenic materials for smart windows or other suitable applications.

In Table 1, the advantages and disadvantages of each route were reported, together with the type of nanoTiO_2 obtained.

Table 1. Synthetic routes, advantages, disadvantages, and morphology of nanoTiO$_2$.

Synthetic Methods	Advantages	Disadvantages	Morphology and Uses	References
Sol-gel	– High yield; – Low temperature; – High control of size and shape of nanoparticles.	– Low purity; – Long post treatment synthesis.	– TiO$_2$NPs (anatase and rutile); – amorphous and crystalline TiO$_2$ thin film EC device; – TiO$_2$ thin films for perovskyte solar cells.	[36–38,42,43,45,46]
Chemical Vapor Deposition (CVD)	– The use of high vacuum is not required; – It permits the covering of rough surfaces uniformly; – The pressures used allow for coating three dimensionally; – The structures have large aspect ratios; – The reactor can be scaled to fit several substrates;	– The source materials used are toxic or flammable, requiring careful management in the design and operation of a CVD process system; – The process requires high temperatures; – The alteration of bond strengths of the precursors provokes some difficulties in controlling stoichiometry.	– TiO$_2$ nanorods; – Amorphous TiO$_2$ films.	[24,48,54,55,102]
Physical Vapor Deposition(PVD)	– The use of specialized precursor materials, as used in CVD, is not required; – A large range of materials (elements, alloys, and compounds) are available for deposition; – The materials are less toxic than those used for CVD. – The sputtering target shows a stable geometry.	– The PVD targets are often expensive; – A degradation of the substrate can occur after radiation and bombardment from the plasma; – The incident energy on the target turns into heat; – In some cases, the flux distribution is not uniform and requires other procedures to adjust the position of the substrates to achieve thin films of uniform thickness.	– Amorphous TiO$_2$ films; – Anatase-phase TiO$_2$ films for electrochromic (EC) devices; – TiO$_2$ nanowires.	[56,58,59,61,67,103,104]

Table 1. *Cont.*

Synthetic Methods	Advantages	Disadvantages	Morphology and Uses	References
Sonochemical and microwave-assisted methods	− The sonochemical reactors show high mass transfer, mixing time, and flow pattern; − High rate of heating; − High rate of cooling; − Generation of shock waves.	− The decline of power with time; − It is not easy to obtain a uniform distribution of ultrasonic energy with an ultrasonic bath; − High frequency of irradiation; − High power consumption.	− anatase, rutile and brookite TiO_2NPs − TiO_2 film	[69,76,78,81,105,106]
Hydrothermal method	− Suitable for creating crystalline phases; − Suitable for materials with high vapor pressure; − It provides well crystallized and pure materials, preventing additional thermal treatments.	− Expensive equipment; − Impossibility of observing the crystal grow; − Autoclaves require 300 °C and 10 bar.	− TiO_2 nanorods − pure anatase and rutile TiO_2	[76,81,83,85,107]
Oxidation method	− TiO_2 nanomaterials are generated in one-step anodization of titanium without any particular pretreatment; − The annealing temperature required is low.	− Use of toxic solvents; − Growth and nucleation steps instability.	− TiO_2 Nanorods − TiO_2 thin film and plate − Rutile TiO_2 nanowires	[87,90,108,109]

Table 1. *Cont.*

Synthetic Methods	Advantages	Disadvantages	Morphology and Uses	References
Spray pyrolysis	− Simple equipment and experimental arrangement; − It does not require the use of high-quality reagents; − The physical properties of particles and films are tuned by varying the preparative conditions, additives, flow rate, and the precursor concentration; − Low-cost; − It permits the achievement of porous and high-density films.	− The yield is very low; − The scale up is difficult; − The sulfides oxidation phenomena can occur in air atmosphere, but there are difficulties with determining the growth temperature.	− TiO_2 thin film for EC devices.	[26,93,110,111]
Green route	− It requires not toxic agents; − Cheap lab equipment; − Possibility to obtain non-toxic nanomaterials.	− The sizes of the nanomaterial are irregular; − The control of crystal growth is low.	− Anatase and rutile TiO_2NPs	[112,113]

2.8. Deposition Techniques: Spin Coating and Doctor Blade

Solutions of titanium diisopropoxide bis(acetylacetonate) and 2-methyloxyethanol with proper values of volume ratio [29] can be deposited by means of simple laboratory methods such as spin-coating and further heating treatment. In general, spin coating is suitable for the fabrication of thin films in order to deposit uniform coatings of materials on flat surfaces by centrifugal force.

This approach allows for the fabrication of both amorphous and anatase structures, according to the heating temperature. Films obtained by chemical solution deposition reported optical modulations of up to 35% for 0.3 μm thick films in visible wavelengths. Mihelčič et al. [111] reported the fabrication of thin (100–400 nm) EC TiO_2 and $Ni_{1−x}O$ coatings. The anatase TiO_2 NPs, having a size ranging from 6 to 10 nm, were dispersed in trisilanol heptaisobutylsilsesquioxane. The obtained dispersion was deposited by spin-coating on glass and plastic (PET) film. In order to obtain the thin film, a thermal treatment was made (150 °C), and it was successively used to obtain foil-based EC devices with transmissive modulation of light. The doctor blade method allows the production of thin films on large surface areas. In a typical doctor blading process, a well-mixed slurry composed of additives and ceramic NPs is deposited on a substrate by meant of a doctor blade. The slurry spreads after a flow is developed between the blade and the substrate; a film layer with a microscale thickness is then formed after drying [114]. Transparent, as-prepared, TiO_2 films were also made by the doctor blade technique, subsequently sintered at 450 °C, and embodied in a *quasi* solid-state EC device [115]. The architecture of such devices utilizes transparent conductive oxide/8.1 μm thick TiO_2/Electrolyte and Polyethylene/Transparent conductive oxide. A transmittance modulation as high as 61.82% was observed, activated by a bias of 3.7 V in 61.8 s.

Dinh et al. [116] developed EC TiO_2 anatase thin transparent films (600 nm of thickness) on F-doped tin oxide (FTO) substrates by the doctor blade technique using TiO_2 NPs (15 nm). The coloration of the devices occurred in $LiClO_4$ solution (1M) showing a CE of 33.7 $cm^2 C^{−1}$ in the visible range.

3. Toxicity Assessment of TiO_2 NPs and Films

The strategies adopted to evaluate the toxicity and the conceivable safety of nanomaterials are the same as those used for conventional drugs [117]. However, nanosized materials exhibit unique physico-chemical properties that require specific methods in order to assess the in vivo response and the uptake effectiveness, drug release, and kinetics [118,119]. So far, no specific protocols have been developed in the preclinical studies, although regulatory institutions from the USA (Food and Drugs Administration, FDA), EU (European Medicines Agency, EMA), and Japan (Pharmaceuticals and Medical Devices Agency, PDMA) are making strong efforts to produce a clear proposition regarding nanomaterial safety [120,121]. The National Center for Advancing Translational Sciences (NCATS/NIH) in the United States and the Innovative Medicines Initiative (IMI) in Europe are the relevant institutions who are aiming to develop regulatory protocols [122]. NPs can enter into living organisms through different routes, which are inhalation, ingestion, and skin penetration. Many in vitro studies have shown the potential toxicity of TiO_2 NPs on different cell lines; these effects are strongly dependent on NP shape, size, aggregation, and crystalline forms. In general, the anatase phase was found to be more toxic than the rutile phase; in addition, the small size and tubular shape were associated to higher TiO_2 toxicity. However, many variables in the safety assessment are introduced by cell line models, which are different in terms of responsiveness, surface receptors, uptake mechanisms, and sensibility due to the activation of different biochemical pathways during the NP exposure time. For this reason, more complete studies devoted to the understanding of toxicity mechanisms are derived from in vivo studies in which it is also possible to study NP distribution in the tissues and organs once they have entered the body. Several studies were performed in order to understand the toxicity of TiO_2 NPs using different animal models and different administration routes. In order to mimic the inhalation process, a micro-syringe was used to administer rutile 500 ug of TiO_2 NPs (80 nm) and anatase (155 nm) every day through the nose of female mice, showing the accumulation in the brain [123]. The authors analyzed the inflammation response and oxidative stress (up to

30 days of exposure) with daily TiO$_2$ NPs administration. The boost of lipid peroxidation induced a strong increase of tumor necrosis factor alpha (TNF-alpha) and interleukin (IL-1 beta), particularly after anatase phase exposure. Additionally, hamsters, rats, and mice treated by TiO$_2$ NPs (P25) for up to 13 weeks showed macrophages and neutrophils activation, followed by strong pulmonary inflammation [124]. The same NPs, at a concentration of 4.1 mg/m^3, were used to treat Wistar rats by aerosol administration for four weeks, and an increase of neutrophils in the bronchoalveolar lavage fluid (BALF) was recorded [125]. TiO$_2$ NPs are also commonly used as white food additives (E171) in a lot of commercial products such as sweets, chewing gums, and puddings [21]; gastro-intestinal accumulation has been studied as well as possible accumulation in several organs. In mice [126], the oral exposure to TiO$_2$ NPs at different concentrations (0, 324, 648, 972, 1296, 1944, 2592 mg/kg) up to 14 days provoked lethargy, loss of appetite, and passive behavior; in addition, accumulation of TiO$_2$ NPs was shown in the liver, kidneys, lungs, and spleen. The latter organ was also investigated in another work, after the administration of TiO$_2$ NPs into the stomach for one month (5, 50, and 150 mg/kg body weight). The spleen underwent a damage and inflammation process due to the activation of a strong lipid peroxidation triggered by ROS production [127]. The ROS production caused the activation of a series of biochemical reactions that induced an unbalance of cell homeostasis, leading to DNA damage [128]. A recent work [129] demonstrated the reduction of the richness and evenness of gut microbiota, with the consequent disruption of gut microbial community compositions in adult mice exposed to TiO$_2$ NPs (50 mg/kg) by intragastric administration for 30 days. Mice presented a reduction in motor activity, even when the memory brain function was not damaged. Li et al. [130] studied the possible alteration of mice gut microbiota structure after oral administration of anatase and rutile TiO$_2$ NPs for 28 days. The concentrations used were the equivalent consumed by candy lovers. NPs were found to accumulate in the spleen, lung, and kidney; an alteration in terms of colon villi length and width were recorded in the intestine (Figure 5). Furthermore, oral administration of two different sizes of TiO$_2$ NPs (260 nm and 66 nm) for 10 days boosted susceptibility of the small intestine portions such as the duodenum, jejunum, and ileum of mice. The portions of organs extracted after the exposure to NPs reported high levels of TiO$_2$ accumulation with a consequent inflammation of several tissues by cytokines activation [131].

TiO$_2$ NPs are also used in the cosmetic and personal care industries, in particular in dermal consumer products such as sunscreens and UV radiation filters [132]. Four pathways of penetration across the skin have been identified depending on the physico-chemical properties of the compound: intercellular, transcellular, and two transappendageal pathways, through hair follicles and sweat glands [133]. The penetration of micro TiO$_2$ NPs in epidermis and dermis is considered highly improbable; microparticles tend to be retained on the outermost surface of the stratum corneum [134]. At the nanoscale level, the situation may be different [135,136] because NPs can cross the derma, especially in the presence of irritations or lesions [137,138]. Numerous in vitro and in vivo studies have been conducted to quantify the penetration rate of TiO$_2$ NPs on both undamaged and injured skin. According to works by Newman et al. [7], a negligible amount of TiO$_2$ NPs penetrated healthy skin; this conclusion was corroborated by Sadrieh et al. [139]. Most of the studies reported so far in the literature deal with the direct exposure of living organisms and cells to TiO$_2$ NPs by different administration methods (oral, intravenous, intranasal, etc.) and incubation, respectively. These routes forecast the use of a NPs suspension, namely a physiological medium in which NPs are dispersed (such as saline buffers or culture medium). However, TiO$_2$ is widely used in the development of devices by the use of several techniques, for different fields, ranging from sensors to solar cells. Structure, concentration, and crystal and grain size are important properties that have to be understood in order to address their use in specific applications. In the case of devices, TiO$_2$ is used to form nanometric or microsized films with unique properties, often associated with other kinds of materials, to build multi layered devices. In this scenario, it is interesting to evaluate their toxicity, which is expected to differ from that observed in the studies reported above for NPs. Some works highlighted the compatibility of rutile and anatase TiO$_2$ surfaces as substrates for the cells grown. Carballo-Vila et al. [140] showed the good

adherence and axonal growth of cultured rat cerebral cortex neurons on rutile surfaces. TiO_2 exhibited the highest degree of biocompatibility in terms of neurite extension observed in spiral ganglion (SG) neuritis, compared with other types of films made of gold or stainless steel [141]. Moreover, regarding hepatic cell lines, it has also been demonstrated that the hepatocytes were viable and metabolically active in long-term culture on rutile and anatase TiO_2 [142,143]. Cervantes et al. [144] used sputtering technique in order to obtain different surface morphology, thickness, and roughness of the anatase and rutile TiO_2 thin films. The roughness ranged from 2.8 to 8.08 nm when the temperature was increased from 300 to 800 °C. The films were used to evaluate the in vitro viability of Chinese Hamster Ovary (CHO-K1) cells after 24, 48, and 72 h of culture. The obtained results indicated that thin films of TiO_2 did not induce adverse effects on CHO-K1 proliferation. The highest cell survival rate was observed in TiO_2 films annealed at 800 °C (Figure 6).
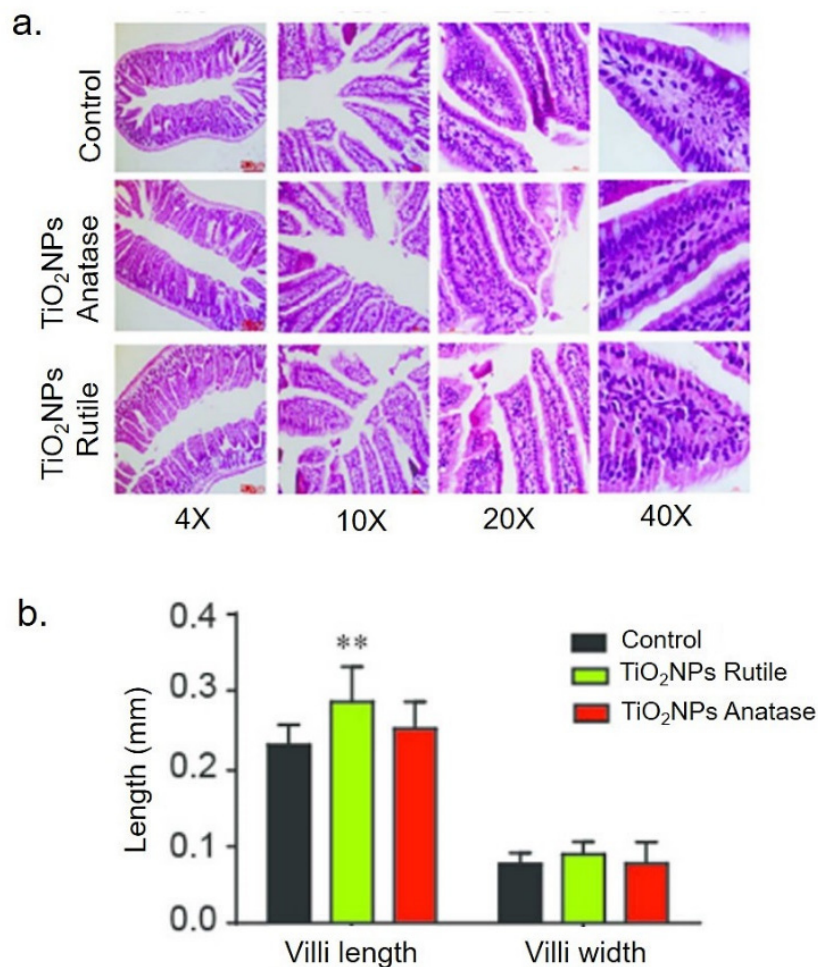
Figure 5. (**a**) Histological acquisitions of mouse colon tissue at different magnifications (4, 10, 20, and 40×) after Hematoxylin and Eosin staining. (**b**) Quantitative intestinal villi length and width ratio analysis. Data were statistically significant for ** $p < 0.05$ compared to the control group. Adapted from [130] with Permission of the Royal Society of Chemistry, Copyright 2018.
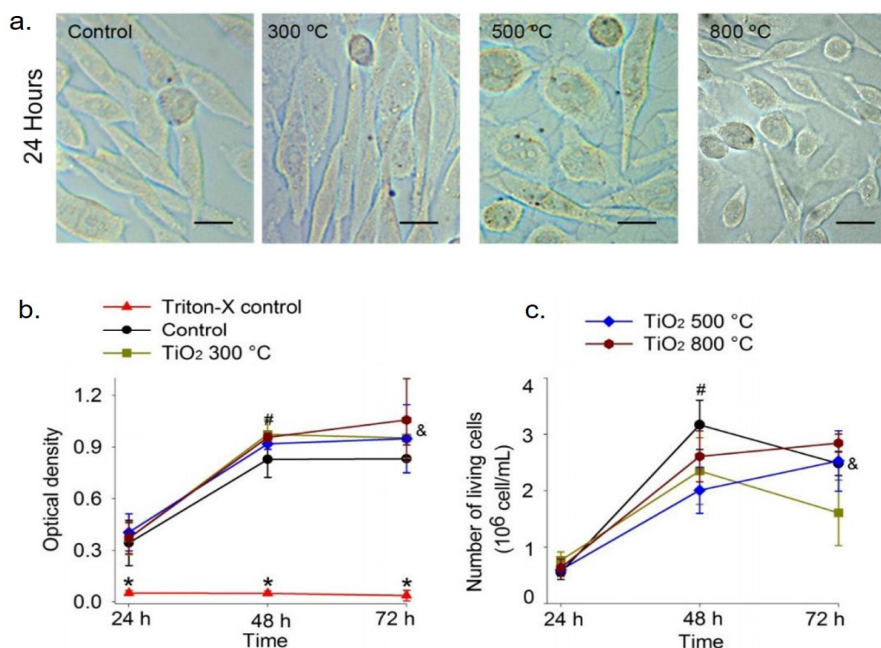
Figure 6. (**a**) Representative optical microscopy images of Chinese Hamster Ovary (CHO-K1) cells cultured on TiO_2 thin films annealed at 300, 500, and 800 °C after 24 h. No significant differences were observed with respect to control. Scale bar = 20 μm for all the images. (**b**) Optical density after 24, 48, and 72 h of Triton-X control (borosilicate glass plus Triton-X), control (borosilicate glass), and TiO_2 films in cells. (**c**) Number of unstained CHO-K1 cells (in millions) on control substrate and on TiO_2 thin films after 24, 48, and 72 h. * Triton X-100 24 h vs. Triton X-100 48 or 72 h; # 24 h vs. 48 h; and & 24 h vs. 72 h. Reprinted from [144].

4. TiO_2 in the Design of Chromogenic Devices—General Considerations

"Smart windows" may represent one of the fields in which TiO_2 may be exploited. It has been shown that the use of windows capable of modulating their spectral characteristics can lead to significant energy savings, on an annual basis, both in terms of electricity consumption for air conditioning and for artificial lighting [145]. An intelligent shielding of incident solar radiation also may enhance indoor visual comfort for occupants. In the following pages, the duel use of TiO_2 in the field of "chromogenics" is shown. TiO_2 can be used as a cathodic material in EC devices, and in photoelectrochromic (PEC) devices—a relatively recent class of multifunctional devices—it can play the role of a photoanode, with the aim of generating electrons by photovoltaic conversion. In our opinion, this particular versatility of TiO_2 deserves further considerations because this field of application could lead to significant energy savings in several sectors, especially transportation and construction. TiO_2 has caught the attention of several research groups working in the field of chromogenics worldwide, who might offer a relevant contribution for limiting energy consumption. The term "chromogenic" indicates the change of optical properties in response to an external stimulus [146]. Such stimuli may be represented by an external bias (in ECs [147]), temperature (in thermochromics [148,149]) or ultraviolet irradiation (in photochromics [150,151]) and oxidizing or reducing gases (in gasochromics [152]). Spectral modulation of optical properties may result in an optimized tuning of the energy flux through glazing, with particular reference to the visible and infrared ranges of the impinging solar radiation. An accurate design and building integration of chromogenics may eventually reduce cooling/heating loads and enhance indoor visual comfort as well [153–156]. Over the last few decades, a strong impulse towards experimental research dealing with TiO_2 has come via nanoscience. This has disclosed unexpected, emerging properties of the materials due to shape and size, affecting interfacial behavior as well as phonon and photon transport, and inverting the surface-to-volume ratio, as reported previously in this work [88,157,158]. Different crystal structures have been reported for TiO_2, such

as anatase [159], brookite [160,161], and rutile [162,163]. In each of them, a TiO_6 octahedron contains Ti^{4+} ions, surrounded by six O^{2-} atoms. Amorphous TiO_2 has shown a larger bandgap compared to anatase, whereas it was found to be narrower for rutile [147]. TiO_2 has been widely adopted as an EC material because it undergoes color modulation due to an external voltage, activating reversible red/ox reactions.

Cathodic TiO_2 films act as intercalation hosts for small cations, (mainly hydrogen or lithium). TiO_2 films are transparent (as-prepared) and turn into absorbing films if the following, reversible redox reactions are activated:

$$TiO_2 + xH^+ + xe^- \leftrightarrow TiO_{2-x}(OH)_x$$

$$TiO_2 + xLi^+ + xe^- \leftrightarrow Li_xTiO_2$$
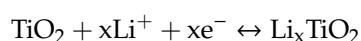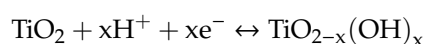
This gives rise to a modulation, generally due to an absorbance contrast, rather than reflectance [164]. In this way, electrons and ions can reach the defect positions of the TiO_2 lattices when a suitable voltage is applied, leading to the colored compound. Such absorbance change has reached 90%, in some cases, throughout the visible and infrared ranges as a consequence of lithium intercalation within the anatase lattice [41]. EC devices generally include more superimposed layers [165]: an electrolyte and two EC materials (anodic and cathodic ones) are sandwiched between two conductive transparent substrates in a "battery-like" architecture (Figure 7). A systematic study dealing with the EC properties of transition metal oxides was reported by C.G. Granqvist [147]. Though tungsten oxide (WO_3) is by far the most investigated EC oxide, TiO_2 is also a widely investigated cathodic coloring material, with a relatively larger coloration time and lower performance compared to WO_3 [42]. Nevertheless, TiO_2 is widely considered a promising candidate for smart windows due to its favorable electrochemical stability, optical modulation, reversibility, low cost preparation, and easy scale up. Compared to WO_3 performance, TiO_2 shows limited CE, higher bias, and slower kinetics [166].
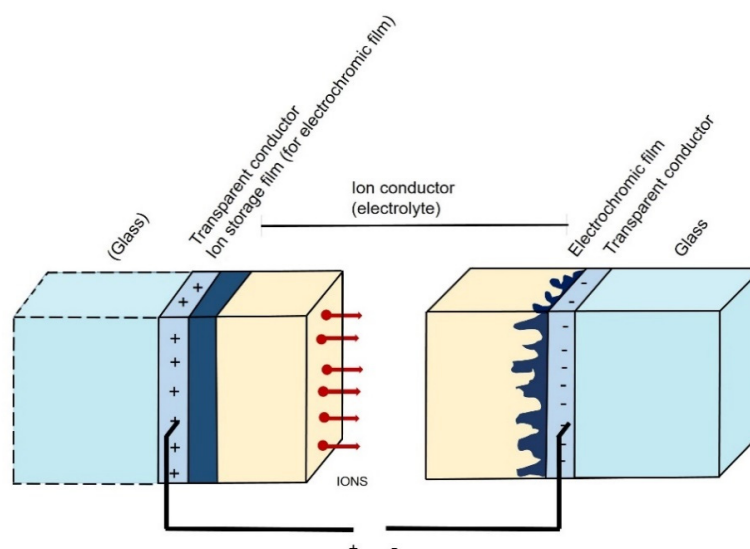
Figure 7. The five-layer stack of a generic EC device, with a "battery-like" architecture.

It is widely recognized that nanosized materials show increased specific surface areas, porosity, and roughness, giving rise, in several cases, to extraordinary physical, chemical, and functional properties [167]. Some groups have reported the EC properties of nanocrystalline TiO_2 films, modified using viologens and anthraquinones [168]. High surface area (80–100 m^2/g) TiO_2 (highly transparent in the as-prepared state) reported a reflectance contrast ratio of 5 at 600 nm [169]. Among TiO_2 polymorphs, the monoclinic-phase TiO_2(B) showed fast lithium intercalation features compared to anatase and rutile due to the more open structure of its crystal lattice. Coloration times of 5 s were observed by Giannuzzi et al. [170] in EC devices fabricated using TiO_2(B) films, with full coloration at

2.0 V. Furthermore, a study by Patil et al., investigating one dimensional (1-D) brookite nanoneedles (650 nm long and 30 nm wide) obtained by hot-filament metal-oxide vapor deposition, reported an optical contrast of 67% [171].

Han et al. [172] presented some TiO_2-doped WO_3 films. Starting from the consideration that mixed WO_3-TiO_2 thin film had a five times longer lifetime than bare WO_3, they prepared amorphous WO_3 thin films, embedding crystalline anatase TiO_2 by dipcoating. The mixing ratio of the two materials was found to strongly affect structural, morphological, and, eventually, the EC performance of films. EC devices were assembled using two electrodes and a Lithium-based liquid electrolyte. They observed that the nanocrystal-doped films showed enhanced ionic and electronic transporting properties and, eventually, better EC performance (higher CE—68 cm^2/C—and modulation of ΔOD up to 0.65—and coloration/bleaching times of just 1 s). These figures were higher than bare WO_3, which showed ΔOD of 0.32, CE of 49 cm^2/C, and a coloration and bleaching time of up to 6 s and 23 s, respectively.

Zhang et al. [43] reported enhanced IR modulation in spin-coated, solgel-based TiO_2 films, assembled with solid hybrid polyelectrolytes. Modulation in the Near Infrared Region (NIR) region (28% at 900 nm) was found to be higher than in the visible wavelength (16% at 560 nm). CE of $79.4 \div 82.7$ cm^2/C was found for 80 nm thick layers. Coloration and bleaching times were 16.1 s and 2.8 s, respectively.

Barawi et al. [173] studied niobium (Nb)-doped TiO_2 colloidal nanocrystals for their wide bandgap and promising plasmonic features. TiO_2 nanocrystals doped with varying amounts of Nb nanoparticles have been used to prepare highly transparent electrodes that can be to be used in NIR-selective EC devices. They fabricated a dual-band EC device with 10% doping concentration of Nb. The device showed complementary switching, according to the external voltage applied. In the $0 \div 3$ V window, modulations of transmittance higher than 64% were measured in the 800–2000 nm range of wavelengths. Upon the application of a higher bias, from 3 V to 4 V, further modulation in the visible region was achieved, driven by lithium intercalation into the TiO_2 anatase structure.

The same group [174] reported further results obtained using Vanadium-modified TiO_2 nanocrystals and nanocrystalline WO_3. Such materials were deposited on several electrodes, so as to obtain a typical battery-like device architecture. WO_3 was finely tuned to control NIR transmittance, with low voltages (about 1.6 V for coloration and 0.5 V for bleaching), whereas V-modified TiO_2 was capable of modulating in the visible region, by applying a voltage of 2.2 V.

A single-step process was proposed to deposit WO_3 nanoplate bundles—by chemical bath deposition—over spray deposited TiO_2 films. Nanoplate bundles were capable of improving the charge transport and to prevent degradation of films.

Such films showed a current density of 3 mA/cm^2 and a stable optical modulation (ΔT) of 78% after 1000 cycles [166].

The recent diffusion of studies regarding TiO_2 as a suitable cathodic EC layer has been reviewed by Maiorov et al. [175]. As is well known, TiO_2 is a cheap and abundant material, is highly compatible with other materials, and is inert. The doping of TiO_2 nanocrystals with metal ions having valence between 5 and 6 (optimal doping of about 10% of Nb, W, Mo, or Ta) allows for the design of nanoparticle absorption due to plasmon resonance.

Wu et al. [44] modified TiO_2 nanoparticles deposited on fluorine-doped tin oxide (FTO) substrates, obtaining a device with reversible three-state optical transformation. TiO_2 particles, with a size of $5 \div 10$ nm, were obtained by dip-coating, with a lifting speed of 3000 μm/s. The main figures observed were a contrast of 57%, coloration and bleaching times of 6 s and 20 s, respectively, and stability after 1500 cycles.

Recent studies show a tendency to exploit the properties of TiO_2 at the nanoscale, with significant effects on the performance of EC devices. For instance, Zhang et al. [176] reported that oxygen vacancies not only confer good near-infrared transmittance modulation, but also improve lithium diffusion. They obtained TiO_2 nanocrystals capable of modulating the infrared and visible light transmittance independently in three distinct modes, with a modulation of 95.5% at 633 nm and 90.5%

at 1200 nm, and fast kinetics. Moreover, they demonstrated that the electrical energy consumed in a coloration/bleaching cycle can be stored in the device in the form of chemical energy; afterwards, such "recycled energy" can be released for local reuse or even uploaded to the electrical grid.

Qu et al. [177] reported the performance of bifunctional electrode-based nanocomposite film based on polyoxotungstate $K_{10}P_2W_{17}O_{61}$ and TiO_2 nanowires, resulting in a combination of electrochromism and energy storage features. The films were fabricated via hydrothermal and self-assembly combination methods. The three dimensional properties of the TiO_2 nanoarrays (favoring ion adsorption and the transport of charges, with a very low resistance) enabled a high CE of 150.34 cm^2/C (at 600 nm), cyclic stability, and a the volumetric capacitance of 172.3 F cm^{-3}.

5. TiO$_2$ in Photoelectrochromic (PEC) and Photovoltachromic Devices

In contrast to EC devices, PEC devices [178] are capable of changing their transmittance properties upon light absorption and do not require any external voltage to produce such effects. The activating stimulus, for PECs, is the impinging light (as in photochromic films) but, in this case, the device absorbs light and generates a sufficient driving force capable of activating the transmittance modulation in an EC material, as described hereafter. Unlike photochromic molecules [150,179,180], which are widely used in solar control lenses where one material hosts light detection and coloration at the same time, the two processes require distinct materials within PEC devices. The first coupling of a TiO_2-based ruthenium polypiridine-sensitized nanocrystalline electrode (acting as a photoanode) with a WO_3 EC counter electrode was proposed by Bechinger et al. in 1996 [181]. In this device architecture, the dye-sensitized TiO_2 played the same role as it does in Grätzel cells [182–184], producing the suitable photovoltage required to color the EC cathodic material deposited on the counter electrode. In fact, TiO_2 indeed plays a different role in PECs, compared to EC devices. In this case, it is of fundamental importance for it to harvest solar energy and convert it into electricity in order to guarantee the operation of a PEC device. Because TiO_2 plays the role of a photoanode, devoted to the photovoltaic generation of electric charge, coloration is generally due to other EC materials, such as WO_3 or poly-(3,4-ethylenedioxythiophene) (PEDOT), which require relatively low photovoltage to undergo full transmittance modulation. This first PEC device, if exposed to sunlight in short-circuit conditions, undergoes a sensible modulation of transmittance because photogenerated electrons are free to move towards the counter electrode via an external circuit. The latter electrode, negatively charged, activates intercalation of small cations from a liquid electrolyte. This phenomenon is then very similar to the intercalation process typically observed in EC devices, resulting in a reversible coloration of WO_3. The physical separation between photogeneration of electrons (on the TiO_2-based photoanode) and electron/ion insertion (on the EC counter electrode) is the reason why Bechinger's device is considered a "separated" architecture for PEC devices (Figure 8, left side). The two electrode substrates are effectively sealed using a Surlyn thermoplastic, leaving an empty space to be filled by means of a liquid electrolyte; generally, this is a solution of iodine ions in propylene carbonate. The ions are used to reduce the dye after its oxidation due to electron generation. Furthermore, a study conducted by Gregg [185], dealing with the same "separated architecture" for PECs, explained that the I_2 typically used in the electrolytes of dye-sensitized cells is decreased in order to maximize both the photovoltage and the transparency of devices. Subsequently, Li et al. [186] used a polyaniline counter electrode instead of the cathodic WO_3. Because the former material shows an anodic behavior, the device was colored in the initial conditions and underwent bleaching if irradiated, in short-circuit conditions. Hsu et al. [187] utilized an organic dye for a TiO_2 photo-electrode; in that case, the EC material adopted was poly(3,3-diethyl-3.4-dihydro-2*H*-thieno-[3,4-b][1,4]dioxepine) (PProDot-Et$_2$). An abrupt change in PEC architectures was proposed by a research group from the German Fraunhofer Institute, who deposited, for the first time, both TiO_2 and the EC layer on the same electrode in a "combined architecture" where PV and EC materials shared the same substrate, which had some interesting effects on the device operation [188–190] (Figure 8 right side). Moreover, a thin transparent platinum layer was deposited on the counter electrode, acting as a catalyzer.
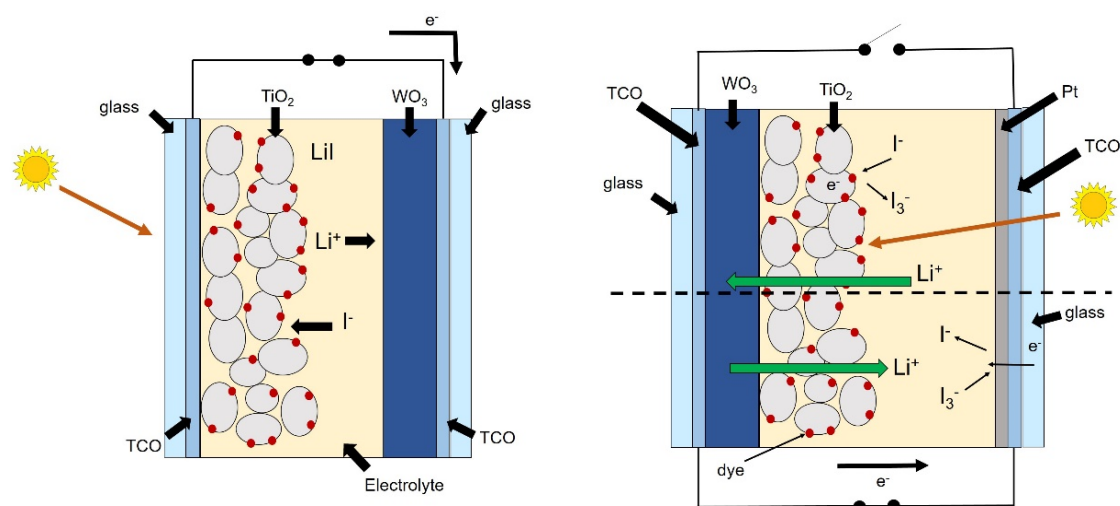
Figure 8. Cross-section of a typical photoelectrochromic (PEC) device with "separated architecture" (**left**). Coloration in open circuit (**upper part**) and bleaching in short circuit (**lower part**) of PEC device with "combined architecture" (**right**).

Such device colored in open-circuit conditions and bleached in the dark, if short-circuited. A modulation of 41% was observed in the full irradiation of devices (1 sun), which took place in a couple of minutes.

Another PEC with a "separated architecture" was proposed by Liao et al. [191], using poly-(3,4-ethylenedioxythiophene) (PEDOT) as a cathodic EC material; the authors observed a CE of 280 cm^2/C and a transmittance modulation of 22% at 630 nm. Krasovec et al. [192] scaled up their PECs (with combined architecture) to dimensions of (10 × 10) cm^2. A solid, ormolyte-based lithium ion conductor was used, combining the electrolytic properties of organic polymers to a strong, inorganic structure; the modulations of visible transmittance reached 63% (Figure 5, right side). A significant step forward in the design of TiO_2-based PECs was proposed by Wu et al. [193], who proposed the first photovoltachromic device, embodying a dye-sensitized frame-type TiO_2 photoanode. The center of the device was transparent and acted as a smart window, changing color depending on the available external irradiance. A photovoltachromic device not only undergoes smart transmittance modulation, like PEC devices, but also provides photovoltaic conversion of solar energy. The fast coloration time observed (as low as 4 s) was accelerated by the platinum catalyst deposited on the counter electrode. This device also allowed for energy harvesting to be delivered to the electric grid. A significant boost in photovoltaic conversion efficiency was reported in 2011 [194], with a photovoltachromic device that reached a fair conversion efficiency (6.55%); the counter electrode was specially designed to allow for a separation of the device features (photovoltaic and PEC), with many circuitries devoted to smart coloration and electricity generation, respectively. Other works appeared, with the same approach, to demonstrate not only the electro-optical figures of merit of such devices, but also the consequent benefits in terms of energy yield and visual comfort [195,196]. A systematic work, dealing with the main figures of merit of PEC devices containing dye-sensitized TiO_2 photoelectrodes, has been reported by the research group of Leftheriotis et al. [197,198]. They also investigated the properties of devices containing poly(methyl methacrylate)-based gel electrolytes [199] and the long-term performance of partly covered devices [200]. A new class of solar cells, based on mixed organic–inorganic halide perovskites [201] has held some significance since 2012. The self-assembly of $CH_3NH_3PbBr_3$ perovskite, within the nanoporous TiO_2 typically used in dye-sensitized cells, had already been studied by Miyasaka et al. [202], who reported a conversion efficiency of 2.19%. In these devices, perovskite acts as a light harvester, replacing the role of dyes in Grätzel cells. Later, it was observed that organic–inorganic halide perovskites could conduct both electrons and holes; this point led to further evolution of perovskite-based PVs towards more simple, planar perovskite solar cells [203,204]. The role

of mesoporous TiO_2, as reported by Park et al. [205], was to assists in the collection of charge carriers, as demonstrated by the efficiency of these cells, reaching 22% in 2016. On the other hand, it was 15.6% in planar cells.

Worldwide, perovskite-based technologies for PVs have attracted the attention of researchers and manufacturers, with the aim of a fast increase of the figures of merit and the commercialization of stable, large-area solar modules without relevant forms of hysteresis. In this roadmap, Eperon et al. [206] demonstrated that perovskite solar cells could be fabricated at room temperature with a significant reduction in the fabrication steps. They also demonstrated that a customized de-wetting of $CH_3NH_3PbI_{3-x}Cl_x$ perovskite after spin-coating may lead to the formation of micro-islands, partially covering the surface to increase the device transparency. In their planar device, a compact TiO_2 layer and a p-type spiro-OMeTAD hole transporter were embodied [206,207]. Such devices allowed a further step forward in the design of photovoltachromic architectures. A multifunctional device, including a semi-transparent perovskite-based PV film, was reported in 2015. It was coupled with an EC material to generate a complex device (Figure 9). The first electrode hosted the semi-transparent PV film (compact TiO_2 was obtained by spin-coating a mildly acidic solution of titanium isopropoxide in ethanol) on one side but was also coated with indium tin oxide (ITO) on the other. The latter acted as one of the electrodes of the EC part of this architecture. The second electrode hosted the cathodic EC material and was "glued" to the first one using a specially designed quasi-solid polymer electrolyte (PEG-plasticized PEO containing lithium iodide) [208]. The PV film supplied electric power, which could drive transmittance modulation until the transient coloration process was complete. Two external circuits connected the photo-anode of the solar cell to the EC electrode and the PV cathode to the secondary electrode of the EC device.
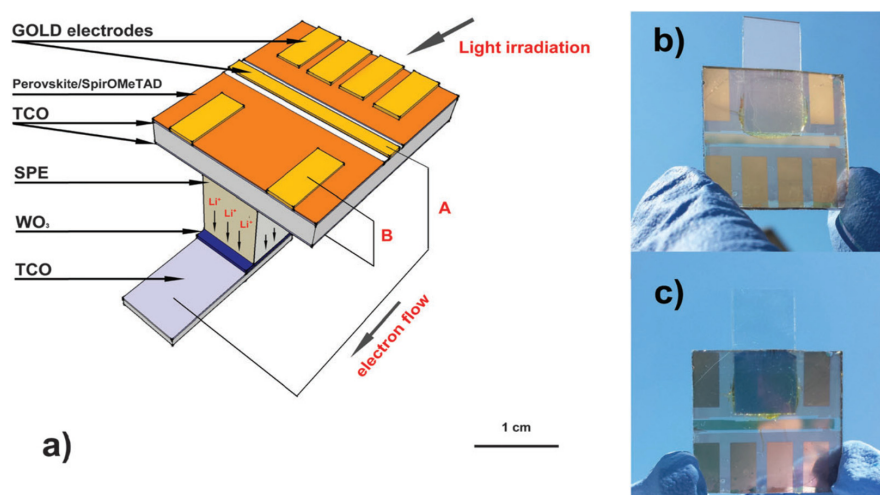
Figure 9. Axonometric view of a perovskite-based photovoltachromic device. Transparent conductive oxides (TCO), solid-state polymer electrolyte (SPE) (**a**). Pictures of the device in bleached (**b**) and colored (**c**) states. Reproduced by permission of The Royal Society of Chemistry [208].

Hocevar et al. [209] scaled up a solid-state device to 30×30 cm^2, which included a dye-sensitized TiO_2 layer, WO_3 as the EC material, and a solid ormolyte electrolyte based on ormosilane within a PEC, thus demonstrating a "combined architecture". All the layers were fabricated by the sol-gel technique and deposited by dip-coating. The T_{vis} modulated spontaneously from 76% to 35% in 15 min under 0.75 sun illumination (750 W/m^2).

Sarwar et al. [210] investigated the applicability of salicylic acid derivatives as suitable dyes for TiO_2 films in PEC devices instead of the typical ruthenium-based sensitizers. They obtained the best results using 5-methylsalicylic acid, observing an optical modulation of 40.8% at 550 nm (Table 2).

Table 2. Fabrication techniques, role of TiO$_2$ and figure of merits of EC devices.

Reference	Fabrication Techniques for TiO$_2$	Role of TiO$_2$	Main Figures of Merit
Nunes et al. [159]	Hydrothermal synthesis assisted by microwave irradiation.	Electrochromic material	ΔR of 57%, 9% and 22% between colored and bleached states, at 250, 550 and 850 nm
Dhandayuthapani et al. [166]	Two step process by combining chemical bath deposition and nebulized spray deposition	Electrochromic material	ΔT of 78%; CE of 128.3 cm^2/C
Choi et al. [168]	Spin-coated nanocrystalline films modified with the viologen from an aqueous solution	Electrochromic material	The absorbance difference at 608 nm between the bleached and colored state of meso-nc-TiO$_2$ EC cell was about 0.43.
Giannuzzi et al. [170]	Surfactant-assisted nonaqueous sol–gel route	Electrochromic material	CE of 130 cm^2/C at 800 nm; coloration time of 5 s
Patil et al. [171]	One dimensional brookite TiO$_2$ nanoneedles coated on glass substrates	Electrochromic material	ΔT of 67% and ΔOD of 0.85
Han et al. [172]	Dip-coating	Electrochromic material	CE of 68 cm^2/C
Barawi et al. [173]	Screen-printing of a Nb-TiO$_2$-containing viscous paste	Electrochromic material	$\Delta T_{NIR} \approx 53\%$, $\Delta T_{MAX} = 67\%$ at 2000 nm at 3 V.
Zhang et al. [176]	Modified nonaqueous fluoride-assisted one-pot method	Electrochromic material	ΔT of 95.4% at 633 nm, 98.7% at 800 nm, 90.5% at 1200 nm, and 76.2% at 1600 nm after 2000 cycles
Qu et al. [177]	Hydrothermal and layer-by-layer self-assembly combination methods	Electrochromic material and energy storage	CE of 150.34 cm^2/C at 600 nm and volumetric capacitance of 172.3 F/cm^{-3}
Bechinger et al. [181]	Dye-sensitized Nanocrystalline TiO$_2$.	Smart coloration according to photogenerated photovoltage	Full modulation in 100 s. Highly reversible after 10^7 cycles.
Hsu et al. [187]	Synthesis of TiO$_2$ nanoparticles as reported for Gratzel cells [182].	Solar energy conversion and photoelectrochromic behavior	ΔT of 33.7%; switching response of 3 s; J$_{SC}$ of 0.89 mA/cm^2 and V$_{OC}$ of 0.57 V
Hauch et al. [188]	Doctor-blading technique using a sol–gel TiO$_2$ paste	Smart coloration according to photogenerated photovoltage	ΔT from 64% to 23% in 2 min
Liao et al. [191]	Dip- coating of a TiO$_2$-containing aqueous suspension, dried in air	Smart coloration according to photogenerated photovoltage	CE of 280 cm^2/C, ΔT of 25%

Table 2. *Cont.*

Reference	Fabrication Techniques for TiO_2	Role of TiO_2	Main Figures of Merit
Wu et al. [193]	Spin-coating of TiO_2 P25 paste	Solar energy conversion and photoelectrochromic behavior	Bleaching time of 4 s at open circuit. Photovoltaic conversion efficiency (η) of 0.46.
Cannavale et al. [194]	Screen-printable paste containing 30 nm sized TiO_2 colloids	Solar energy conversion and photoelectrochromic behavior	η of 6.55; ΔOD of 0.83 at 780 nm
Leftheriotis et al. [197]	Doctor blade technique	Smart coloration according to photogenerated photovoltage	ΔT of 36%; coloration time of 12 min.
Cannavale et al. [208]	Spin-coating of a mildly acidic solution of titanium isopropoxide in ethanol	Solar energy conversion and photoelectrochromic behavior	Average visible transmittance of 26%; η of 5.5%
Hočevar et al. [209]	Sol-gel processing	Smart coloration according to photogenerated photovoltage	ΔT of 41% in 15 min
Sarwar et al. [210]	Doctor blade technique	Smart coloration according to photogenerated photovoltage	ΔT of 40.8% at 550 nm

6. Conclusions

Recent trends in the field of chromogenics demonstrate a renewed interest in the applications of TiO_2. In particular, from the examination reported here, though not exhaustive, the emergence of a wide number of investigations dealing with this material in the nanoscale, mainly in the form of nanoparticles and nanotubes, can be observed. The combination of TiO_2 with other EC materials (especially WO_3) has recently made it possible to obtain enhanced performances that are of significant interest. Additionally, the use in PEC devices represents another area of interest that includes the use of TiO_2 within the wider field of multifunctional devices.

In this review, the main characteristics of TiO_2 have been reported, with special reference to their morphological, structural, chemical, and physical properties. These characteristics have been related to the main synthetic routes for NPs and to the process fabrication of thin films. One paragraph was entirely dedicated to a rapid, though non exhaustive, review of the state-of-the-art regarding TiO_2 toxicity, both in the form of NPs and in thin films, with specific regard to the current international regulatory framework. Therefore, the EC properties of TiO_2 have been discussed, reporting the main studies concerning its use as a cathodic EC material in devices and as a sensitized photoelectrode in PEC and photovoltachromic devices. This work aims to highlight the potential use of TiO_2 for the purposes of energy saving, exploiting its ease of deposition and the consolidated knowledge of its properties, synthesis, and deposition systems.

Author Contributions: Conceptualization, V.D.M. and A.C.; writing—original draft preparation, U.A., V.D.M. and A.C.; writing—review and editing, U.A., V.D.M. and A.C. All authors have read and agreed to the published version of the manuscript.

Conflicts of Interest: The authors declare no conflict of interest.

References

1. Shukla, R.K.; Sharma, V.; Pandey, A.K.; Singh, S.; Sultana, S.D.A. ROS-mediated genotoxicity induced by titanium dioxide nanoparticles in human epidermal cells. *Toxicol In Vitro* **2011**, *25*, 231–241. [CrossRef]
2. Szymańska, R.; Kołodziej, K.; Ślesak, I.; Zimak-Piekarczyk, P.; Orzechowska, A.; Gabruk, M.; Żądło, A.; Habina, I.; Knap, W.; Burda, K.; et al. Titanium dioxide nanoparticles (100–1000 mg/L) can affect vitamin E response in Arabidopsis thaliana. *Environ. Pollut.* **2016**, *213*, 957–965. [CrossRef]
3. Nam, Y.; Lim, J.H.; Ko, K.C.; Lee, J.Y. Photocatalytic activity of TiO_2 nanoparticles: A theoretical aspect. *Chin. J. Catal.* **2009**, *30*, 839–851. [CrossRef]
4. Weir, A.; Westerhoff, P.; Fabricius, L.; Hristovski, K.; Von Goetz, N. Titanium dioxide nanoparticles in food and personal care products. *Environ. Sci. Technol.* **2012**, *46*, 2242–2250. [CrossRef]
5. Jameel, N.; Imad, H. Review on: Titanium Dioxide Applications. *Energy Procedia* **2019**, *157*, 17–29. [CrossRef]
6. Stark, W.J.; Stoessel, P.R.; Wohlleben, W.; Hafner, A. Industrial applications of nanoparticles. *Chem. Soc. Rev.* **2015**, *44*, 5793–5805. [CrossRef] [PubMed]
7. Newman, M.D.; Stotland, M.E.J. The safety of nanosized particles in titanium dioxide- and zinc oxide-based sunscreens. *J. Am. Acad. Dermatol.* **2009**, *61*, 685–692. [CrossRef] [PubMed]
8. Friedmann, D.; Mendive, C.; Bahnemann, D. TiO_2 for water treatment: Parameters affecting the kinetics and mechanisms of photocatalysis. *Appl. Catal. B Environ.* **2010**, *99*, 398–406. [CrossRef]
9. Zhang, X.; Jin, M.; Liu, Z.; Tryk, D.A.; Nishimoto, S.; Murakami, T.; Fujishima, A. Superhydrophobic TiO_2 Surfaces: Preparation, Photocatalytic Wettability Conversion, and Superhydrophobic−Superhydrophilic Patterning. *J. Phys. Chem. C* **2007**, *111*, 14521–14529. [CrossRef]
10. Ma, Y.; Wang, X.; Jia, Y.; Chen, X.; Han, H.; Li, C. Titanium Dioxide-Based Nanomaterials for Photocatalytic Fuel Generations. *Chem. Rev.* **2014**, *114*, 9987–10043. [CrossRef]

11. Rahimi, N.; Pax, R.A.; Gray, E.M. Review of functional titanium oxides. I: TiO₂ and its modifications. *Prog. Solid State Chem.* **2016**, *44*, 86–105. [CrossRef]

12. Li, M.; Yin, J.J.; Wamer, W.G.; Lo, Y.M. Mechanistic characterization of titanium dioxide nanoparticle-induced toxicity using electron spin resonance. *J. Food Drug Anal.* **2014**, *22*, 76–85. [CrossRef] [PubMed]

13. Reyes-Coronado, D.; Rodríguez-Gattorno, G.; Espinosa-Pesqueira, M.E.; Cab, C.; de Coss, R.D.; Oskam, G. Phase-pure TiO₂ nanoparticles: Anatase, brookite and rutile. *Nanotechnology* **2008**, *19*, 145605. [CrossRef] [PubMed]

14. Bourikas, K.; Kordulis, C.; Lycourghiotis, A. Titanium Dioxide (Anatase and Rutile): Surface Chemistry, Liquid–Solid Interface Chemistry, and Scientific Synthesis of Supported Catalysts. *Chem. Rev.* **2014**, *114*, 9754–9823. [CrossRef] [PubMed]

15. Oi, L.E.; Choo, M.Y.; Lee, H.V.; Ong, H.C.; Abd Hamid, S.B.; Juan, J.C. Recent advances of titanium dioxide (TiO2) for green organic synthesis. *Rsc. Adv.* **2016**, *6*, 108741–108754. [CrossRef]

16. Photocatalysis on TiO₂ Surfaces: Principles, Mechanisms, and Selected Results. *Chem. Rev.* **1995**, *95*, 735–758. [CrossRef]

17. Ola, O.; Maroto-Valer, M.M. Review of material design and reactor engineering on TiO₂ photocatalysis for CO2 reduction. *J. Photochem. Photobiol. C Photochem. Rev.* **2015**, *24*, 16–42. [CrossRef]

18. Fujishima, A.; Honda, K. Electrochemical Photolysis of Water at a Semiconductor Electrode. *Nature* **1972**, *238*, 37–38. [CrossRef]

19. Adachi, M.; Murata, Y.; Okada, I.; Yoshikawa, S. Formation of titania nanotubes and applications for dye-sensitized solar cells. *J. Elelectrochem. Soc.* **2003**, *150*, G488–G493. [CrossRef]

20. Kang, S.H.; Choi, S.H.; Kang, M.S.; Kim, J.Y.; Kim, H.S.; Hyeon, T.; Sung, Y.E. Nanorod-Based Dye-Sensitized Solar Cells with Improved Charge Collection Efficiency. *Adv. Mater.* **2007**, *20*, 54–58. [CrossRef]

21. De Matteis, V.; Rinaldi, R. Toxicity Assessment in the Nanoparticle Era. In *Cellular and Molecular Toxicology of Nanoparticles. Advances in Experimental Medicine and Biology*; Springer: Cham, Switzerland, 2018; pp. 1–19.

22. Ahn, K.H.; Park, Y.B.; Park, D.W. Kinetic and mechanistic study on the chemical vapor deposition of titanium dioxide thin films by in situ FT-IR using TTIP. *Surface Coat. Technol.* **2003**, *171*, 198–204. [CrossRef]

23. Shi, J.; Wang, X. Growth of Rutile Titanium Dioxide Nanowires by Pulsed Chemical Vapor Deposition. *Cryst. Growth Des.* **2011**, 949–954. [CrossRef]

24. Fictorie, C.P.; Evans, J.F.; Gladfelter, W.L. Kinetic and mechanistic study of the chemical vapor deposition of titanium dioxide thin films using tetrakis (isopropoxo) titanium (IV). *J. Vac. Sci. Technol. A* **1998**, *12*, 1108–1113. [CrossRef]

25. Nyamukamba, P.; Okoh, O.; Mungondori, H.; Taziwa, R.; Zinya, S. Synthetic Methods for Titanium Dioxide Nanoparticles: A Review. In *Titanium Dioxide—Material for a Sustainable Environment*; Yang, D., Ed.; BoD–Books on Demand: Norderstedt, Germany, 2018; pp. 151–175. [CrossRef]

26. Natarajan, C.; Fukunaga, N.; Nogami, G. Titanium dioxide thin film deposited by spray pyrolysis of aqueous solution. *Thin Solid Film.* **2005**, 6–8. [CrossRef]

27. Okuya, M.; Nakade, K.; Kaneko, S. Porous TiO₂ thin films synthesized by a spray pyrolysis deposition (SPD) technique and their application to dye-sensitized solar cells. *Solar Energy Mater. Solar Cells* **2002**, *70*, 425–435. [CrossRef]

28. Conde-gallardo, A.; Guerrero, M.; Castillo, N.; Soto, A.B. TiO₂ anatase thin films deposited by spray pyrolysis of an aerosol of titanium diisopropoxide. *Thin Solid Film.* **2005**, *473*, 68–73. [CrossRef]

29. Kursawe, M.; Anselmann, R.; Hilarius, V.; Pfaff, G.; Kgaa, M.; Optics, D.P.; Strasse, M. Nano-Particles by Wet Chemical Processing in Commercial Applications. *J. Sol-Gel Sci. Technol.* **2005**, 71–74. [CrossRef]

30. Gupta, S.K.; Desai, R.; Jha, P.K.; Kirin, D.; Wiley, J. Titanium dioxide synthesized using titanium chloride: Size effect study using Raman spectroscopy and photoluminescence. *J. Raman Spectrosc.* **2010**, *2009*, 350–355. [CrossRef]

31. Kontos, A.I.; Kontos, A.G.; Tsoukleris, D.S.; Bernard, M.C.; Spyrellis, N.; Falaras, P. Nanostructured TiO₂ films for DSSCS prepared by combining doctor-blade and sol–gel techniques. *J. Mater. Proc. Technol.* **2008**, *196*, 243–248. [CrossRef]

32. Rosseinsky, D.R.; Mortimer, R.J. *Electrochromic Materials and Devices*; Mortimer, R.J., Rosseinsky, D.R., Monk, P.M.S., Eds.; Wiley-VCH Verlag GmbH & Co. KGaA: Weinheim, Germany, 2013; ISBN 9783527679850.

33. Gour, A.; Jain, N.K. Advances in green synthesis of nanoparticles. *Artif. Cells Nanomed. Biotechnol.* **2019**, *47*, 844–851. [CrossRef]

34. Brinker, C.J.; Scherer, G. *Sol-Gel Science: The Physics and Chemistry of Sol-Gel Processing*; Academic Press: New York, NY, USA, 2013.

35. Oskam, G.; Nellore, A.; Penn, R.L.; Searson, P.C. The growth kinetics of TiO_2 nanoparticles from titanium (IV) alkoxide at high water/titanium ratio. *J. Phys. Chem. B* **2003**, *107*, 1734–1738. [CrossRef]

36. Mehrotra, R.C.; Singh, A. Recent trends in metal alkoxide chemistry. *Prog. Inorg. Chem.* **1997**, *46*, 239–454.

37. Danks, A.E.; Hall, S.R.; Schnepp, Z.J. The evolution of "sol–gel" chemistry as a technique for materials synthesis. *Mater. Horiz.* **2016**, *3*, 91–112. [CrossRef]

38. Jeffrey Brinker, C.; Scherer, G.W. (Eds.) *Sol–Gel Science, the Physics and Chemistry of Sol–Gel Processing*; Academic Press: Cambridge, MA, USA, 1990; 924p, ISBN 0-12-134970-5.

39. Brinker, C.J.; Hurd, A.J.; Schunk, P.R.; Frye, G.C.; Ashley, C.S. Review of sol-gel thin film formation. *J. Non-Cryst. Solids* **1992**, *147–148*, 424–436. [CrossRef]

40. Nabavi, M.; Doeuff, S.; Sanchez, C.; Livage, J. Sol-gel synthesis of electrochromic films. *Mater. Sci. Eng. B* **1989**, *3*, 203–207. [CrossRef]

41. Chen, X.; Mao, S.S. Titanium dioxide nanomaterials: Synthesis, properties, modifications and applications. *Chem. Rev.* **2007**, *107*, 2891–2959. [CrossRef]

42. Dinh, N.N.; Oanh, N.T.T.; Long, P.D.; Bernard, M.C.; Goff, A.H. Le Electrochromic properties of TiO_2 anatase thin films prepared by a dipping sol-gel method. *Thin Solid Film.* **2003**, *423*, 70–76. [CrossRef]

43. Zhang, B.; Xu, C.; Xu, G.; Tan, S.; Zhang, J. Amorphous titanium dioxide film with improved electrochromism in near-infrared region. *Opt. Mater.* **2019**, *89*, 191–196. [CrossRef]

44. Wu, L.; Yang, D.; Fei, L.; Huang, Y.; Wu, F.; Sun, Y.; Shi, J.; Xiang, Y. Dip-Coating Process Engineering and Performance Optimization for Three-State Electrochromic Devices. *Nanoscale Res. Lett.* **2017**, *12*, 1–15. [CrossRef]

45. Muthee, D.K.; Dejene, B.F. The effect of tetra isopropyl orthotitanate (TIP) concentration on structural, and luminescence properties of titanium dioxide nanoparticles prepared by sol-gel method. *Mater. Sci. Semicond. Process.* **2020**, *106*, 104783. [CrossRef]

46. Singh, R.; Ryu, I.; Yadav, H.; Park, J.; Jo, J.W.; Yim, S.; Lee, J.J. Non-hydrolytic sol-gel route to synthesize TiO_2 nanoparticles under ambient condition for highly efficient and stable perovskite solar cells. *Sol. Energy* **2019**, *185*, 307–314. [CrossRef]

47. Nateq, M.H.; Ceccato, R. Sol-Gel Synthesis of TiO_2 Nanocrystalline Particles with Enhanced Surface Area through the Reverse Micelle Approach. *Adv. Mater. Sci. Eng.* **2019**, 1567824. [CrossRef]

48. Gurav, A.S.; Kodas, T.T.; Wang, L.M.; Kauppinen, E.I.; Joutsensaari, J. Generation of nanometer-size fullerene particles via vapor condensation. *Chem. Phys. Lett.* **1994**, *218*, 304–308. [CrossRef]

49. Maria Benelmekki, A.E. Nanostructured thin films–background, preparation and relation to the technological revolution of the 21st century. In *Frontiers of Nanoscience*; Elsevier Ltd.: Amsterdam, The Netherlands, 2019; pp. 1–34.

50. Peter, M. Martin Deposition Technologies: An Overview. In *Handbook of Deposition Technologies for Films and Coatings (Third Edition) Science, Applications and Technology*; William Andrew Publishing: Norwich, NY, USA, 2010; pp. 1–31.

51. Shamim Ahmad Organic semiconductors for device applications: Current trends and future prospects. *J. Polym. Eng.* **2014**, *34*, 279–338. [CrossRef]

52. Johnson, R.W.; Hultqvist, A.; Bent, S.F. A brief review of atomic layer deposition: From fundamentals to applications. *Mater. Today* **2014**, *17*, 236–246. [CrossRef]

53. Seifried, S.; Winterer, M.; Hahn, H. Nanocrystalline Titania films and particles by chemical vapor synthesis. *Chem. Vap. Depos.* **2000**, *6*, 239–244. [CrossRef]

54. Pradhan, S.K.; Reucroft, P.J.; Yang, F.; Dozier, A. Growth of TiO_2 Nanorods by Metalorganic Chemical Vapor Deposition. *J. Cryst. Growth* **2003**, *256*, 83–88. [CrossRef]

55. Wu, J.J.; Yu, C.C. Aligned TiO_2 Nanorods and Nanowalls. *J. Phys. Chem. B* **2004**, *108*, 3377–3379. [CrossRef]

56. Macwan, D.P.; Balasubramanian, C.; Dave, P.N.; Chaturvedi, S. Thermal plasma synthesis of nanotitania and its characterization. *J. Saudi Chem. Soc.* **2014**, *18*, 234–244. [CrossRef]

57. Wu, J.M.; Shih, H.C.; Wu, W.T.; Tseng, Y.K.; Chen, I.C. Thermal evaporation growth and the luminescence property of TiO_2 nanowires. *J. Cryst. Growth* **2005**, *281*, 384–390. [CrossRef]

58. Wu, J.M.; Shih, H.C.; Wu, W.T. Electron field emission from single crystalline TiO_2 nanowires prepared by thermal evaporation. *Chem. Phys. Lett.* **2005**, *413*, 490. [CrossRef]

59. Qiang Zhang, C.L. High Temperature Stable Anatase Phase Titanium Dioxide Films Synthesized by Mist Chemical Vapor Deposition. *Nanomaterials* **2020**, *10*, 911. [CrossRef] [PubMed]

60. Milton Ohring Thin-Film Evaporation Processes. In *Materials Science of Thin Films (Second Edition) Deposition and Structure*; Elsevier: Amsterdam, The Netherlands, 2002; pp. 95–144.

61. Shahidi, S.; Moazzenchi, B.; Ghorannevis, M. A review-application of physical vapor deposition (PVD) and related methods in the textile industry. *Eur. Phys. J. Appl. Phys.* **2015**, *71*, 31302. [CrossRef]

62. Donald, M. Mattox Atomistic Film Growth and Some Growth-Related Film Properties. In *Handbook of Physical Vapor Deposition (PVD) Processing (Second Edition)*; William Andrew: Norwich, NY, USA, 2010; pp. 333–398.

63. Abegunde, O.O.; Akinlabi, E.T.; Oladijo, O.P.; Akinlabi, S.; Ude, A.U. Overview of thin film deposition techniques. *Aims Mater. Sci.* **2019**, *6*, 174–199. [CrossRef]

64. Wasa, K.; Kitabatake, M.; Adachi, H. *Thin Film Materials Technology: Sputtering of Control Compound Materials*; Springer: Berlin/Heidelberg, Germany, 2004.

65. Wasa, K.; Hayakawa, S. *Handbook of Sputter Deposition Technology*; Noyes Publications; William Andrew: Norwich, NY, USA, 1992.

66. Seyfert, U.; Heisig, U.; Teschner, G.; Strümpfel, J. 40 Years of Industrial Magnetron Sputtering in Europe. *Svc. Bull. Fall* **2015**, 22–26.

67. Sorar, I.; Pehlivan, E.; Niklasson, G.A.; Granqvist, C.G. Electrochromism of DC magnetron sputtered TiO_2 thin films: Role of deposition parameters. *Sol. Energy Mater. Sol. Cells* **2013**, *115*, 172–180. [CrossRef]

68. Sorar, I.; Pehlivan, E.; Niklasson, G.A.; Granqvist, C.G. Electrochromism of DC magnetron-sputtered TiO_2: Role of film thickness. *Appl. Surf. Sci.* **2014**, *318*, 24–27. [CrossRef]

69. Gregory Chatel Sonochemistry in nanocatalysis: The use of ultrasound from the catalyst synthesis to the catalytic reaction. *Curr. Opin. Green Sustain. Chem.* **2019**, *15*, 1–6. [CrossRef]

70. Kasap, S.; Tel, H.; Piskin, S. Preparation of TiO_2 nanoparticles by sonochemical method, isotherm, thermodynamic and kinetic studies on the sorption of strontium. *J. Radioanal. Nucl. Chem.* **2011**, *289*, 489–495. [CrossRef]

71. Okitsu, K.; Yue, A.; Tanabe, S.; Matsumoto, H.; Yobiko, Y. Formation of colloidal gold nanoparticles in an ultrasonic field: Control of rate of gold (iii) reduction and size of formed gold particles. *Langmuir ACS J. Surf. Colloids* **2001**, *17*, 7717–7720. [CrossRef]

72. Suslick, K.S.; Didenko, Y.; Fang, M.M.; Hyeon, T.; Kolbeck, K.J.; McNamara, W.B., III; Mdleleni, M.M.; Wong, M. Acoustic cavitation and its chemical consequences. *Phil. Trans. Roy. Soc. A* **1999**, *357*, 335–353. [CrossRef]

73. Gupta, M.; Eugene, W.W.L. Microwaves—Theory. In *Microwaves and Metals*; John Wiley & Sons (Asia) Pte Ltd.: Singapore, 2011; pp. 25–41.

74. Rao, K.J.; Vaidhyanathan, B.; Ganguli, M.; Ramakrishnan, P.A. Synthesis of inorganic solids using microwaves. *Chem. Mater.* **1999**, *11*, 882–895. [CrossRef]

75. Zhu, Y.J.; Chen, F. Microwave-assisted preparation of inorganic nanostructures in liquid phase. *Chem. Rev.* **2014**, *114*, 6462–6555. [CrossRef] [PubMed]

76. Baldassari, S.; Komarneni, S.; Mariani, E.; Villa, C. Rapid microwave–hydrothermal synthesis of anatase form of titanium dioxide. *J. Am. Ceram. Soc.* **2005**, *88*, 3238. [CrossRef]

77. Cabello, G.; Davoglio, R.A.; Pereira, E.C. Microwave-assisted synthesis of anatase-TiO_2 nanoparticles with catalytic activity in oxygen reduction. *J. Electroanal. Chem.* **2017**, *794*, 36–42. [CrossRef]

78. Delgado, L.P.; Figueroa-Torres, M.Z.; Ceballos-Chuc, M.C.; García-Rodríguez, R.; Alvarado-Gil, J.J.; Oskam, G.; Rodriguez-Gattorno, G. Tailoring the TiO_2 phases through microwave-assisted hydrothermal synthesis: Comparative assessment of bactericidal activity. *Mater. Sci. Eng. C* **2020**, *117*, 111290. [CrossRef]

79. Reeja-Jayan, B.; Harrison, K.L.; Yang, K.; Wang, C.L.; Yilmaz, A.E.; Manthiram, A. Microwave-assisted Low-temperature Growth of Thin Films in Solution. *Sci. Rep.* **2012**, *2*, 1003. [CrossRef]

80. Dahiya, M.S.; Tomer, V.K.; Duhan, S. Metal–ferrite nanocomposites for targeted drug delivery. In *Delivery, Applications of Nanocomposite Materials in Drug Biomaterials, Woodhead Publishing Series in Biomaterials*; Woodhead Publishing: Cambridge, UK, 2018; pp. 737–760.

81. Reddy, K.M.; Guin, D.; Manorama, S.V.; Reddy, A.R. Selective synthesis of nanosized TiO_2 by hydrothermal route: Characterization, structure property relation, and photochemical application. *J. Mater. Res.* **2004**, *19*, 2567–2575. [CrossRef]

82. Kim, C.S.; Moon, B.K.; Park, J.H.; Choi, B.C.; Seo, H.J. Solvothermal synthesis of nanocrystalline TiO_2 in toluene with surfactant. *J. Cryst. Growth* **2003**, *257*, 309–315. [CrossRef]

83. Feng, X.; Zhai, J.; Jiang, L. The fabrication and switchable superhydrophobicity of TiO_2 nanorod films. *Angew. Chem. Int. Edition.* **2005**, *44*, 5115–5118. [CrossRef]

84. Stride, J.A.; Tuong, N.T. Controlled synthesis of titanium dioxide nanostructures. *Solid State Phenom.* **2010**, *162*, 261–274. [CrossRef]

85. Maheswari, P.; Ponnusamy, S.; Harish, S.; Ganesh, M.R.; Hayakawa, Y. Hydrothermal synthesis of pure and bio modified TiO_2: Characterization, evaluation of antibacterial activity against gram positive and gram negative bacteria and anticancer activity against KB Oral cancer cell line. *Arab. J. Chem.* **2020**, *13*, 3484–3497. [CrossRef]

86. Beyer, J.; Mamakhel, A.; Søndergaard-Pedersen, F.; Yu, J.; Iversen, B.B. Continuous flow hydrothermal synthesis of phase pure rutile TiO_2 nanoparticles with a rod-like morphology. *Nanoscale* **2020**, *12*, 2695–2702. [CrossRef] [PubMed]

87. Malekshahi Byranvand, M.; Nemati Kharat, A.; Fatholahi, L.; Malekshahi Beiranvand, Z. A Review on Synthesis of Nano-TiO_2 via Different Methods. *J. Nanostruct.* **2013**, *3*, 1–9.

88. Xiaobo, C. Titanium dioxide nanomaterials and their energy applications. *Chin. J. Catal.* **2009**, *30*, 839–851.

89. Rahmat, S.T.; Tan, W.K.; Kawamura, G.; Matsuda, A.; Lockman, Z. Synthesis of rutile TiO_2 nanowires by thermal oxidation of titanium inthe presence of KOH and their ability to photoreduce Cr(VI) ions. *J. Alloy Compd.* **2020**, 152094. [CrossRef]

90. Arcadipane, E.; Sanz, R.; Amiard, G.; Boninelli, S.; Impellizzeri, G.; Privitera, V.; Bonkerud, J.; Bhoodoo, C.; Vines, L.; Svensson, B.G.; et al. Single-crystal TiO_2 nanowires by seed assisted thermal oxidation of Ti foil: Synthesis and photocatalytic properties. *RSC Adv.* **2016**, *6*, 55490–55498. [CrossRef]

91. Gavrilović, T.V.; Jovanović, D.J.; Dramićanin, M.D. Synthesis of Multifunctional Inorganic Materials: From Micrometer to Nanometer Dimensions. In *Nanomaterials for Green Energy-Micro and Nano Technologies*; Elsevier: Amsterdam, The Netherlands, 2018; pp. 55–81.

92. Perednis, D.; Gauckler, L.J. Thin Film Deposition Using Spray Pyrolysis. *J. Electroceram.* **2005**, 103–111. [CrossRef]

93. Ramadhan, Z.R.; Yun, C.; Park, B.I.; Yu, S.; Kang, M.H.; Kim, S.; Lim, D.; Choi, B.H.; Han, J.W.; Kim, Y.H. High performance electrochromic devices based on WO_3eTiO_2 nanoparticles synthesized by flame spray pyrolysis. *Opt. Mater.* **2019**, *89*, 559–562. [CrossRef]

94. Wang, W.N.; Lenggoro, I.W.; Terashi, Y.; Kim, T.O.; Okuyama, K. One-step synthesis of titanium oxide nanoparticles by spray pyrolysis of organic precursors. *Mater. Sci. Eng. B* **2005**, *23*, 194–202. [CrossRef]

95. Abou-Helal, M.O.; Seeber, W.T. Preparation of TiO_2 thin films by spray pyrolysis to be used as a photocatalyst. *Appl. Surf. Sci.* **2002**, *195*, 53–62. [CrossRef]

96. Xu, C.; Zhan, Y.; Hong, K.; Wang, G. Growth and mechanism of titania nanowires. *Solid State Commun.* **2003**, *126*, 545–549. [CrossRef]

97. Subhapriya, S.; Gomathipriya, P. Green synthesis of titanium dioxide (TiO_2) nanoparticles by Trigonella foenum-graecum extract and its antimicrobial properties. *Microb. Pathog.* **2018**, *116*, 215–220. [CrossRef] [PubMed]

98. Thakur, B.K.; Kumar, A.; Kumar, D. Green synthesis of titanium dioxide nanoparticles using Azadirachta indica leaf extract and evaluation of their antibacterial activity. *S. Afr. J. Bot.* **2019**, *124*, 223–227. [CrossRef]

99. Sundrarajan, M.; Gowri, S. Green synthesis of titanium dioxide nanoparticles by Nyctanthes arbor-tristis leaves extract. *Chalcogenide Lett.* **2011**, *8*, 447–451.

100. Roopan, S.M.; Bharathi, A.; Prabhakarn, A.; Rahuman, A.A.; Velayutham, K.; Rajakumar, G.; Padmaja, R.D.; Lekshmi, M.; Madhumitha, G. Efficient phyto-synthesis and structural characterization of rutile TiO_2 nanoparticles using Annona squamosa peel extract. *Spectrochim Acta Part A* **2012**, *98*, 86–90. [CrossRef]

101. Renata Dobrucka Synthesis of Titanium Dioxide Nanoparticles Using Echinacea purpurea Herba. *Iran. J. Pharm. Res.* **2017**, *16*, 756–762.

102. Angus Rockett Chemical Vapor Deposition. In *The Materials Science of Semiconductors*; Springer: Boston, MA, USA, 2008.

103. Donald, M. *Mattox Handbook of Physical Vapor Deposition (PVD) Processing*; Noyes Publications; William Andrew: Westwood, NJ, USA, 1998; ISBN 978-0-81-552037-5.

104. De Matteis, V.; Cannavale, A.; Blasi, L.; Quarta, A.; Gigli, G. Chromogenic device for cystic fibrosis precocious diagnosis: A "point of care" tool for sweat test. *Sens. Actuators B Chem.* **2016**, *225*, 474–480. [CrossRef]

105. Asgharzadehahmadi, S.; Raman, A.A.; Parthasarathy, R.; Sajjadi, B. Sonochemical reactors: Review on features, advantages and limitations. *Renew. Sustain. Energy Rev.* **2016**, *63*, 302–314. [CrossRef]

106. Tang, Y.; Wang, F.; Jin, C.; Liang, H.; Zhong, X.; Yang, Y. Mitochondrial Injury Induced by Nanosized Titanium Dioxide in A549 Cells and Rats. *Environ. Toxicol. Pharmacol.* **2013**, *36*, 66–72. [CrossRef]

107. Ulrich Schubert, N.H. *Synthesis of Inorganic Materials*, 4th ed.; Wiley-VCH Verlag GmbH & Co. KGaA: Weinheim, Germany, 2019; ISBN 978-3-527-34457-4.

108. Su, Z.; Zhang, L.; Jiang, F.; Hong, M. Formation of crystalline TiO2 by anodic oxidation of titanium. *Prog. Nat. Sci. Mater. Int.* **2013**, *23*, 294–301. [CrossRef]

109. Varghese, O.K.; Gong, D.; Paulose, M.; Grimes, C.A.; Dickey, E.C. Crystallization and high temperature structural stability of titanium oxide nanotube arrays. *J. Mater. Res.* **2003**, *18*, 156–165. [CrossRef]

110. Leng, J.; Wang, Z.; Wang, J.; Wu, H.H.; Yan, G.; Li, X.; Guo, H.; Liu, Y.; Zhang, Q.; Guo, Z. Advances in nanostructures fabricated via spray pyrolysis and their applications in energy storage and conversion. *Chem. Soc. Rev.* **2019**, *48*, 3015–3072. [CrossRef] [PubMed]

111. Mihelčič, M.; Jerman, I.; Orel, B. Preparation of electrochromic Ni1−xO and TiO$_2$ coatings from pigment dispersions and their application in electrochromic foil based devices. *Prog. Org. Coat.* **2013**, *76*, 1752–1755. [CrossRef]

112. Nadeem, M.; Tungmunnithum, D.; Hano, C.; Abbasi, B.H.; Hashmi, S.S.; Ahmad, W.; Zahir, A. The current trends in the green syntheses of titanium oxide nanoparticles and their applications. *Green Chem. Lett. Rev.* **2018**, *11*, 492–502. [CrossRef]

113. Rana, A.; Yadav, K.; Jagadevan, S. A comprehensive review on green synthesis of nature-inspired metal nanoparticles: Mechanism, application and toxicity. *J. Clean. Prod.* **2020**, *272*, 122880. [CrossRef]

114. Aegerter, M.A.; Mennig, M. (Eds.) *Sol-Gel Technologies for Glass Producers and Users*; Springer: Boston, MA, USA, 2004.

115. Sarangika, H.N.M.; Dissanayake, M.A.K.L.; Senadeera, G.K.R.; Karunarathne, W.G.M.D. Low cost quasi solid state electrochromic devices based on F-doped tin oxide and TiO$_2$. *Mater. Today Proc.* **2019**, *23*, 100–104. [CrossRef]

116. Dinh, N.N.; Quyen, N.M.; Zikova, M.; Truong, V.V. Highly-efficient electrochromic performance of nanostructured TiO$_2$ films made by doctor blade technique. *Sol. Energy Mater. Sol. Cells* **2011**, *95*, 618–623. [CrossRef]

117. Dobrovolskaia, M.A.; McNeil, S.E. Understanding the correlation between in vitro and in vivo immunotoxicity tests for nanomedicines. *J. Control Release* **2013**, *172*, 456–466. [CrossRef]

118. De Matteis, V. Exposure to Inorganic Nanoparticles: Routes of Entry, Immune Response, Biodistribution and In Vitro/In Vivo Toxicity Evaluation. *Toxics* **2017**, *5*, 29. [CrossRef]

119. De Matteis, V.; Cascione, M.; Toma, C.C.; Leporatti, S. Morphomechanical and organelle perturbation induced by silver nanoparticle exposure. *J. Nanopart Res.* **2018**, *20*, 273. [CrossRef]

120. Mühlebach, S.; Borchard, G.; Yildiz, S. Regulatory challenges and approaches to characterize nanomedicines and their follow-on similars. *Nanomedicine* **2015**, *10*, 659–674. [CrossRef] [PubMed]

121. Wagner, V.; Dullaart, A.; Bock, A.K.; Zweck, A. The emerging nanomedicine landscape. *Nat. Biotechnol.* **2006**, *24*, 1211–1217. [CrossRef] [PubMed]

122. Gupta, R.; Xie, H. Nanoparticles in Daily Life: Applications, Toxicity and Regulations. *J. Environ. Pathol. Toxicol. Oncol.* **2018**, *37*, 209–230. [CrossRef] [PubMed]

123. Wang, J.; Liu, Y.; Jiao, F.; Lao, F.; Li, W.; Gu, Y.; Li, Y.; Ge, C.; Zhou, G.; Li, B.; et al. Time-dependent translocation and potential impairment on central nervous system by intranasally instilled TiO$_2$ nanoparticles. *Toxicology* **2008**, *5*, 82–90. [CrossRef] [PubMed]

124. Bermudez, E.; Mangum, J.B.; Wong, B.A.; Asgharian, B.; Hext, P.M.; Warheit, D.B.; Everitt, J.I. Pulmonary Responses of Mice, Rats, and Hamsters to Subchronic Inhalation of Ultrafine Titanium Dioxide Particles. *Toxicol. Sci.* **2004**, *357*, 347–357. [CrossRef]

125. Okada, T.; Lee, B.W.; Ogami, A.; Oyabu, T.; Myojo, T. Inhalation of titanium dioxide (P25) nanoparticles to rats and changes in surfactant protein (SP-D) levels in bronchoalveolar lavage fluid and serum. *Toxicology* **2019**, *13*, 1396–1408. [CrossRef]

126. Chen, J.; Dong, X.; Zhao, J.; Tang, G. In vivo acute toxicity of titanium dioxide nanoparticles to mice after intraperitioneal injection. *J. Appl. Toxicol.* **2009**, *29*, 330–337. [CrossRef]

127. Wang, J.; Li, N.; Zheng, L.; Wang, S.; Wang, Y.; Zhao, X.; Duan, Y.; Cui, Y.; Zhou, M.; Cai, J.; et al. P38-Nrf-2 signaling pathway of oxidative stress in mice caused by nanoparticulate TiO$_2$. *Biol. Trace Elem. Res.* **2011**, *140*, 186–197. [CrossRef]

128. Mohamed, H.R. Estimation of TiO$_2$ nanoparticle-induced genotoxicity persistence and possible chronic gastritis-induction in mice. *Food Chem. Toxicol.* **2015**, *83*, 76–83. [CrossRef]

129. Zhang, S.; Jiang, X.; Cheng, S.; Fan, J.; Qin, X.; Wang, T.; Zhang, Y.; Zhang, J.; Qiu, Y.; Qiu, J.; et al. Titanium dioxide nanoparticles via oral exposure leads to adverse disturbance of gut microecology and locomotor activity in adult mice. *Arch. Toxicol.* **2020**, 1–18. [CrossRef] [PubMed]

130. Li, J.; Yang, S.; Lei, R.; Gu, W.; Qin, Y.; Ma, S.; Chen, K.; Chang, Y.; Bai, X.; Xia, S.; et al. Oral administration of rutile and anatase TiO$_2$ nanoparticles shifts mouse gut microbiota structure. *Nanoscale* **2018**, *10*, 7736–7745. [CrossRef] [PubMed]

131. Nogueira, C.M.; de Azevedo, W.M.; Dagli, M.L.; Toma, S.H.; de Arruda Leite, A.Z.; Lordello, M.L.; Nishitokukado, I.; Ortiz-Agostinho, C.L.; Duarte, M.I.; Ferreira, M.A.; et al. Titanium dioxide induced inflammation in the small intestine. *World J. Gastroenterol.* **2012**, *18*, 4729–4735. [CrossRef] [PubMed]

132. Robertson, T.A.; Sanchez, W.Y.; Roberts, M.S. Are commercially available nanoparticles safe when applied to the skin? *J. Biomed. Nanotechnol.* **2010**, *6*, 452–468. [CrossRef] [PubMed]

133. Crosera, M.; Prodi, A.; Mauro, M.; Pelin, M.; Florio, C. Titanium Dioxide Nanoparticle Penetration into the Skin and Effects on HaCaT Cells. *Int. J. Environ. Res. Public Health* **2015**, 9282–9297. [CrossRef]

134. Schulz, J.; Hohenberg, H.; Pflücker, F.; Gärtner, E.; Will, T.; Pfeiffer, S.; Wepf, R.; Wendel, V.; Gers-Barlag, H.; Wittern, K.P. Distribution of sunscreens on skin. *Adv. Drug Deliv. Rev.* **2002**, *54*, 157–163. [CrossRef]

135. Lademann, J.; Weigmann, H.J.; Rickmeyer, C.; Barthelmes, H.; Schaefer, H.; Mueller, G.; Sterry, W. Penetration of Titanium Dioxide Microparticles in a Sunscreen Formulation into the Horny Layer and the Follicular Orifice. *Ski. Pharm. Appl. Ski. Physiol.* **1999**, *12*, 247–256. [CrossRef]

136. Senzui, M.; Tamura, T.; Miura, K.; Ikarashi, Y.; Watanabe, Y.; Fujii, M. Study on penetration of titanium dioxide (TiO($_2$)) nanoparticles into intact and damaged skin in vitro. *J. Toxicol. Sci.* **2010**, *35*, 107–113. [CrossRef]

137. Wu, J.; Liu, W.; Xue, C.; Zhou, S.; Lan, F.; Bi, L.; Xu, H.; Yang, X.; Zeng, F.D. Toxicity and penetration of TiO$_2$ nanoparticles in hairless mice and porcine skin after subchronic dermal exposure. *Toxicol. Lett.* **2009**, *191*, 1–8. [CrossRef]

138. Bennat, C.; Müller-Goymann, C.C. Müller-Goymann Skin penetration and stabilization of formulations containing microfine titanium dioxide as physical UV filter. *Int. J. Cosmet. Sci.* **2001**, *22*, 271–283. [CrossRef]

139. Sadrieh, N.; Wokovich, A.M.; Gopee, N.V.; Zheng, J.; Haines, D.; Parmiter, D.; Siitonen, P.H.; Cozart, C.R.; Patri, A.K.; McNeil, S.E.; et al. Lack of significant dermal penetration of titanium dioxide from sunscreen formulations containing nano- and submicron-size TiO$_2$ particles. *Toxicol. Sci.* **2010**, *155*, 156–166. [CrossRef] [PubMed]

140. Carballo-Vila, M.; Moreno-Burriel, B.; Chinarro, E.; Jurado, J.R.; Casañ-Pastor, N.; Collazos-Castro, J.E. Titanium oxide as substrate for neural cell growth. *J. Biomed. Mater. Res. A* **2009**, *90*, 94–105. [CrossRef] [PubMed]

141. Brors, D.; Aletsee, C.; Schwager, K.; Mlynski, R.; Hansen, S.; Schäfers, M.; Ryan, A.F.; Dazert, S. Interaction of spiral ganglion neuron processes with alloplastic materials in vitro(1). *Hear. Res.* **2002**, *167*, 110–121. [CrossRef]

142. Buchloh, S.; Stieger, B.; Meier, P.J.; Gauckler, L. Hepatocyte performance on different crystallographic faces of rutile. *Biomaterials* **2003**, *24*, 2605–2610. [CrossRef]

143. Baranowska-Wójcik, E.; Szwajgier, D.; Oleszczuk, P.; Winiarska-Mieczan, A. Effects of Titanium Dioxide Nanoparticles Exposure on Human Health—A Review. *Biol. Trace Elem. Res.* **2020**, *193*, 118–129. [CrossRef] [PubMed]

144. Cervantes, B.; López-Huerta, F.; Vega, R.; Hernández-Torres, J.; García-González, L.; Salceda, E.; Herrera-May, A.L.; Soto, E. Cytotoxicity Evaluation of Anatase and Rutile TiO$_2$ Thin Films on CHO-K1 Cells in Vitro. *Materials* **2016**, *9*, 619. [CrossRef] [PubMed]

145. Cannavale, A.; Ayr, U.; Fiorito, F.; Martellotta, F. Smart electrochromic windows to enhance building energy efficiency and visual comfort. *Energies* **2020**, *13*, 1449. [CrossRef]

146. Granqvist, C.G.; Lansåker, P.C.; Mlyuka, N.R.; Niklasson, G.A.; Avendaño, E. Progress in chromogenics: New results for electrochromic and thermochromic materials and devices. *Sol. Energy Mater. Sol. Cells* **2009**, *93*, 2032–2039. [CrossRef]

147. Granqvist, C.G. *Handbook of Inorganic Electrochromic Materials*; Elsevier: Amsterdam, The Netherlands, 1995; ISBN 0444899308.

148. Cao, X.; Chang, T.; Shao, Z.; Xu, F.; Luo, H.; Jin, P. Challenges and Opportunities toward Real Application of VO2-Based Smart Glazing. *Matter* **2020**, *2*, 862–881. [CrossRef]

149. Karlessi, T.; Santamouris, M. Improving the performance of thermochromic coatings with the use of UV and optical filters tested under accelerated aging conditions. *Int. J. Low-Carbon Technol.* **2015**, *10*, 45–61. [CrossRef]

150. Cipolloni, M.; Heynderickx, A.; Maurel, F.; Perrier, A.; Jacquemin, D.; Siri, O.; Ortica, F.; Favaro, G. Multiswitchable acidichromic and photochromic bisdiarylethene. An experimental and theoretical study. *J. Phys. Chem. C* **2011**, *115*, 23096–23106. [CrossRef]

151. Arbab, S.; Matusiak, B.S. Toward colour rendering method of window glass. *Color Res. Appl.* **2019**, *44*, 34–43. [CrossRef]

152. Baetens, R.; Jelle, B.P.; Gustavsen, A. Properties, requirements and possibilities of smart windows for dynamic daylight and solar energy control in buildings: A state-of-the-art review. *Sol. Energy Mater. Sol. Cells* **2010**, *94*, 87–105. [CrossRef]

153. Wen, R.T.; Arvizu, M.A.; Niklasson, G.A.; Granqvist, C.G. Electrochromics for energy efficient buildings: Towards long-term durability and materials rejuvenation. *Surf. Coat. Technol.* **2015**, *278*, 121–125. [CrossRef]

154. Granqvist, C.G. Electrochromics for smart windows: Oxide-based thin films and devices. *Thin Solid Film.* **2014**, *564*, 1–38. [CrossRef]

155. Granqvist, C.G.; Bayrak Pehlivan, İ.; Niklasson, G.A. Electrochromics on a roll: Web-coating and lamination for smart windows. *Surf. Coat. Technol.* **2018**, *336*, 133–138. [CrossRef]

156. Granqvist, C.G.; Azens, A.; Heszler, P.; Kish, L.B.; Österlund, L. Nanomaterials for benign indoor environments: Electrochromics for "smart windows", sensors for air quality, and photo-catalysts for air cleaning. *Sol. Energy Mater. Sol. Cells* **2007**, *91*, 355–365. [CrossRef]

157. Hossain, K.; Rameeja, S. Importance of Nanotechnology in Civil Engineering. *Eur. J. Sustain. Dev.* **2015**, *4*, 161–166. [CrossRef]

158. Papadakis, D.; Diamantopoulou, A.; Pantazopoulos, P.A.; Palles, D.; Sakellis, E.; Boukos, N.; Stefanou, N.; Likodimos, V. Nanographene oxide-TiO2 photonic films as plasmon-free substrates for surface-enhanced Raman scattering. *Nanoscale* **2019**, *11*, 21542–21553. [CrossRef]

159. Nunes, D.; Freire, T.; Barranger, A.; Matias, M.; Pereira, S.; Pimentel, A.; Cordeiro, N.J.A.; Fortunato, E.; Martins, R. TiO2 Nanostructured Films for Electrochromic Paper Based-Devices. *Appl. Sci.* **2020**, *10*, 1200. [CrossRef]

160. Pigeot-Rémy, S.; Gregori, D.; Hazime, R.; Hérissan, A.; Guillard, C.; Ferronato, C.; Cassaignon, S.; Colbeau-Justin, C.; Durupthy, O. Size and shape effect on the photocatalytic efficiency of TiO2 brookite. *J. Mater. Sci.* **2019**, *54*, 1213–1225. [CrossRef]

161. Sharma, S.; Venkata Dhanunjaya Reddy, A.; Jayarambabu, N.; Vikram Manoj Kumar, N.; Saineetha, A.; Venkateswara Rao, K.; Kailasa, S. Synthesis and characterization of Titanium dioxide nanopowder for various energy and environmental applications. *Mater. Today Proc.* **2019**, 3–6. [CrossRef]

162. Granqvist, C.G. Electrochromic oxides: A bandstructure approach. *Sol. Energy Mater. Sol. Cells* **1994**, *32*, 369–382. [CrossRef]

163. Granqvist, C.G. Electrochromic oxides: A unified view. *Solid State Ion.* **1994**, *70–71*, 678–685. [CrossRef]

164. Jelle, B.P. Electrochromic Smart Windows for Dynamic Daylight and Solar Energy Control in Buildings. In *Electrochromic Materials and Devices*; Mortimer, R.J., Rosseinsky, D.R., Paul, M.S., Eds.; Monk Wiley-VCH: Hoboken, NJ, USA, 2015; pp. 419–502.

165. Granqvist, C.G.; Arvizu, M.A.; Pehlivan, B.; Qu, H.Y.; Wen, R.T.; Niklasson, G.A. Electrochromic materials and devices for energy efficiency and human comfort in buildings: A critical review. *Electrochim. Acta* **2018**, *259*, 1170–1182. [CrossRef]

166. Dhandayuthapani, T.; Sivakumar, R.; Zheng, D.; Xu, H.; Ilangovan, R.; Sanjeeviraja, C.; Lin, J. WO$_3$/TiO$_2$ hierarchical nanostructures for electrochromic applications. *Mater. Sci. Semicond. Process.* **2020**, 2–7. [CrossRef]

167. Yang, G.; Zhang, Y.M.; Cai, Y.; Yang, B.; Gu, C.; Zhang, S.X. Advances in nanomaterials for electrochromic devices. *Chem. Soc. Rev.* **2020**, *49*, 8687–8720. [CrossRef]

168. Sung, Y.C.; Mamak, M.; Coombs, N.; Chopra, N.; Ozin, G.A. Electrochromic performance of viologen-modified periodic mesoporous nanocrystalline anatase electrodes. *Nano Lett.* **2004**, *4*, 1231–1235. [CrossRef]

169. Vlachopoulos, N.; Nissfolk, J.; Möller, M.; Briançon, A.; Corr, D.; Grave, C.; Leyland, N.; Mesmer, R.; Pichot, F.; Ryan, M.; et al. Electrochemical aspects of display technology based on nanostructured titanium dioxide with attached viologen chromophores. *Electrochim. Acta* **2008**, *53*, 4065–4071. [CrossRef]

170. Giannuzzi, R.; Manca, M.; De Marco, L.; Belviso, M.R.; Cannavale, A.; Sibillano, T.; Giannini, C.; Cozzoli, P.D.; Gigli, G. Ultrathin TiO$_2$(B) nanorods with superior lithium-ion storage performance. *ACS Appl. Mater. Interfaces* **2014**, *6*, 1933–1943. [CrossRef]

171. Patil, R.A.; Devan, R.S.; Liou, Y.; Ma, Y.R. Efficient electrochromic smart windows of one-dimensional pure brookite TiO2 nanoneedles. *Sol. Energy Mater. Sol. Cells* **2016**, *147*, 240–245. [CrossRef]

172. Han, J.; Ko, K.W.; Sarwar, S.; Lee, M.S.; Park, S.; Hong, S.; Han, C.H. hwan Enhanced electrochromic properties of TiO$_2$ nanocrystal embedded amorphous WO$_3$ films. *Electrochim. Acta* **2018**, *278*, 396–404. [CrossRef]

173. Barawi, M.; De Trizio, L.; Giannuzzi, R.; Veramonti, G.; Manna, L.; Manca, M. Dual Band Electrochromic Devices Based on Nb-Doped TiO$_2$ Nanocrystalline Electrodes. *ACS Nano* **2017**, *11*, 3576–3584. [CrossRef]

174. Barawi, M.; Veramonti, G.; Epifani, M.; Giannuzzi, R.; Sibillano, T.; Giannini, C.; Rougier, A.; Manca, M. A dual band electrochromic device switchable across four distinct optical modes. *J. Mater. Chem. A* **2018**, *6*, 10201–10205. [CrossRef]

175. Maiorov, V.A. Electrochromic Glasses with Separate Regulation of Transmission of Visible Light and Near-Infrared Radiation (Review). *Opt. Spectrosc.* **2019**, *126*, 412–430. [CrossRef]

176. Zhang, S.; Cao, S.; Zhang, T.; Lee, J.Y. Plasmonic Oxygen-Deficient TiO$_2$-x Nanocrystals for Dual-Band Electrochromic Smart Windows with Efficient Energy Recycling. *Adv. Mater.* **2020**, *32*, 2–9. [CrossRef]

177. Qu, X.; Fu, Y.; Ma, C.; Yang, Y.; Shi, D.; Chu, D.; Yu, X. Bifunctional electrochromic-energy storage materials with enhanced performance obtained by hybridizing TiO$_2$ nanowires with POMs. *New J. Chem.* **2020**, *44*, 15475–15482. [CrossRef]

178. Cannavale, A.; Cossari, P.; Eperon, G.E.; Colella, S.; Fiorito, F.; Gigli, G.; Snaith, H.J.; Listorti, A. Forthcoming perspectives of photoelectrochromic devices: A critical review. *Energy Environ. Sci.* **2016**, *9*, 2682–2719. [CrossRef]

179. Ke, Y.; Chen, J.; Lin, G.; Wang, S.; Zhou, Y.; Yin, J.; Lee, P.S.; Long, Y. Smart Windows: Electro-, Thermo-, Mechano-, Photochromics, and Beyond. *Adv. Energy Mater.* **2019**, *9*, 1–38. [CrossRef]

180. Ortica, F. The role of temperature in the photochromic behaviour. *Dye Pigment* **2012**, *92*, 807–816. [CrossRef]

181. Bechinger, C.; Ferrere, S.; Zaban, A.; Sprague, J.; Gregg, B.A. Photoelectrochromic windows and displays. *Nature* **1996**, *383*, 608–610. [CrossRef]

182. O'Regan, B.; Gratzel, M. A Low-Cost, High-Efficiency Solar-Cell Based on Dye-Sensitized Colloidal TiO$_2$ Films. *Nature* **1991**, *353*, 737–740. [CrossRef]

183. Huang, S.Y.; Schlichthörl, G.; Nozik, A.J.; Grätzel, M.; Frank, A.J. Charge recombination in dye-sensitized nanocrystalline TiO$_2$ solar cells. *J. Phys. Chem. B* **1997**, *101*, 2576–2582. [CrossRef]

184. Parisi, M.L.; Maranghi, S.; Basosi, R. The evolution of the dye sensitized solar cells from Grätzel prototype to up-scaled solar applications: A life cycle assessment approach. *Renew. Sustain. Energy Rev.* **2014**, *39*, 124–138. [CrossRef]

185. Gregg, B.A. Photoelectrochromic applications. *Endeavour* **1997**, *21*, 52–55. [CrossRef]

186. Li, Y.; Hagen, J.; Haarer, D. Novel photoelectrochromic cells containing a polyaniline layer and a dye-sensitized nanocrystalline TiO$_2$ photovoltaic cell. *Synth. Met.* **1998**, *94*, 273–277. [CrossRef]

187. Hsu, C.Y.; Lee, K.M.; Huang, J.H.; Justin Thomas, K.R.; Lin, J.T.; Ho, K.C. A novel photoelectrochromic device with dual application based on poly(3,4-alkylenedioxythiophene) thin film and an organic dye. *J. Power Sources* **2008**, *185*, 1505–1508. [CrossRef]

188. Hauch, A.; Georg, A.; Baumgärtner, S.; Opara Krašovec, U.; Orel, B. New photoelectrochromic device. *Electrochim. Acta* **2001**, *46*, 2131–2136. [CrossRef]

189. Hauch, A.; Georg, A.; Opara Krašovec, U.; Orel, B. Comparison of photoelectrochromic devices with different layer configurations. *J. Electrochem. Soc.* **2002**, *149*, H159–H163. [CrossRef]

190. Georg, A.; Georg, A.; Opara Krašovec, U. Photoelectrochromic window with Pt catalyst. *Thin Solid Film.* **2006**, *502*, 246–251. [CrossRef]

191. Liao, J.Y.; Ho, K.C. A photoelectrochromic device using a PEDOT thin film. *J. New Mater. Electrochem. Syst.* **2005**, *8*, 37–47.

192. Krašovec, U.O.; Georg, A.; Georg, A.; Wittwer, V.; Luther, J.; Topič, M. Performance of a solid-state photoelectrochromic device. *Sol. Energy Mater. Sol. Cells* **2004**, *84*, 369–380. [CrossRef]

193. Wu, J.J.; Hsieh, M.D.; Liao, W.P.; Wu, W.T.; Chen, J.S. Fast-switching photovoltachromic cells with tunable transmittance. *ACS Nano* **2009**, *3*, 2297–2303. [CrossRef] [PubMed]

194. Cannavale, A.; Manca, M.; Malara, F.; De Marco, L.; Cingolani, R.; Gigli, G. Highly efficient smart photovoltachromic devices with tailored electrolyte composition. *Energy Environ. Sci.* **2011**, *4*, 2567–2574. [CrossRef]

195. Cannavale, A.; Manca, M.; De Marco, L.; Grisorio, R.; Carallo, S.; Suranna, G.P.; Gigli, G. Photovoltachromic device with a micropatterned bifunctional counter electrode. *ACS Appl. Mater. Interfaces* **2014**, *6*, 2415–2442. [CrossRef]

196. Malara, F.; Cannavale, A.; Carallo, S.; Gigli, G. Smart windows for building integration: A new architecture for photovoltachromic devices. *ACS Appl. Mater. Interfaces* **2014**, *6*, 9290–9297. [CrossRef]

197. Leftheriotis, G.; Syrrokostas, G.; Yianoulis, P. Development of photoelectrochromic devices for dynamic solar control in buildings. *Sol. Energy Mater. Sol. Cells* **2010**, *94*, 2304–2313. [CrossRef]

198. Leftheriotis, G.; Syrrokostas, G.; Yianoulis, P. Partly covered photoelectrochromic devices with enhanced coloration speed and efficiency. *Sol. Energy Mater. Sol. Cells* **2012**, *96*, 86–92. [CrossRef]

199. Theodosiou, K.; Dokouzis, A.; Antoniou, I.; Leftheriotis, G. Gel electrolytes for partly covered photoelectrochromic devices. *Sol. Energy Mater. Sol. Cells* **2019**, *202*, 110124. [CrossRef]

200. Dokouzis, A.; Theodosiou, K.; Leftheriotis, G. Assessment of the long-term performance of partly covered photoelectrochromic devices under insolation and in storage. *Sol. Energy Mater. Sol. Cells* **2018**, *182*, 281–293. [CrossRef]

201. Green, M.A.; Ho-Baillie, A.; Snaith, H.J. The emergence of perovskite solar cells. *Nat. Photonics* **2014**, *8*, 506–514. [CrossRef]

202. Kojima, A.; Teshima, K.; Shirai, Y.; Miyasaka, T. Novel Photoelectrochemical Cell with Mesoscopic Electrodes Sensitized by Lead-halide Compounds (11). *Meet. Abstr.* **2008**, *MA2008-02*, 27.

203. You, J.; Hong, Z.; Yang, Y.M.; Chen, Q.; Cai, M.; Song, T.; Chen, C.; Lu, S.; Liu, Y.; Zhou, H.; et al. Low-Temperature Solution-Processed Perovskite Solar Cells with High Efficiency and Flexibility. *ACS Nano* **2014**, *8*, 1674–1680. [CrossRef] [PubMed]

204. Eperon, G.E.; Stranks, S.D.; Menelaou, C.; Johnston, M.B.; Herz, L.M.; Snaith, H.J. Formamidinium lead trihalide: A broadly tunable perovskite for efficient planar heterojunction solar cells. *Energy Environ. Sci.* **2014**, *7*, 982. [CrossRef]

205. Park, N.-G.; Grätzel, M.; Miyasaka, T.; Zhu, K.; Emery, K. Towards stable and commercially available perovskite solar cells. *Nat. Energy* **2016**, *1*, 16152. [CrossRef]

206. Eperon, G.E.; Burlakov, V.M.; Goriely, A.; Snaith, H.J. Neutral color semitransparent microstructured perovskite solar cells. *ACS Nano* **2014**, *8*, 591–598. [CrossRef]

207. Hörantner, M.T.; Nayak, P.K.; Mukhopadhyay, S.; Wojciechowski, K.; Beck, C.; McMeekin, D.; Kamino, B.; Eperon, G.E.; Snaith, H.J. Shunt-Blocking Layers for Semitransparent Perovskite Solar Cells. *Adv. Mater. Interfaces* **2016**, *3*, 1–7. [CrossRef]

208. Cannavale, A.; Eperon, G.E.; Cossari, P.; Abate, A.; Snaith, H.J.; Gigli, G. Perovskite photovoltachromic cells for building integration. *Energy Environ. Sci.* **2015**, *8*, 1578–1584. [CrossRef]

209. Hočevar, M.; Opara Krašovec, U. A photochromic single glass pane. *Sol. Energy Mater. Sol. Cells* **2018**, *186*, 111–114. [CrossRef]

210. Sarwar, S.; Park, S.; Dao, T.T.; Lee, M.; Ullah, A.; Hong, S.; Han, C.H. Scalable photoelectrochromic glass of high performance powered by ligand attached TiO$_2$ photoactive layer. *Sol. Energy Mater. Sol. Cells* **2020**, *210*, 110498. [CrossRef]

Publisher's Note: MDPI stays neutral with regard to jurisdictional claims in published maps and institutional affiliations.